ORIGINAL PAPER

Application of airborne laser scanning and electrical resistivity tomography in the study of an active landslide and geology of the cliff, Jastrzębia Góra, Poland

Mirosław Kamiński[1] **· Piotr Zientara**[1] **· Mirosław Krawczyk**[1]

Abstract

The cliff in Jastrzębia Góra is one of the most an active landslide areas along the Polish Baltic coast. The aim of these studies was to determine the dynamics of displacements in an active landslide and to identify the geology of the cliff. Two methods, ALS (Airborne Laser Scanning) and ERT (Electrical Resistivity Tomography), were used for this purpose. Multitemporal ALS data were used to determine the geomorphological changes within the cliff and find the causes of the rapid rate of cliff edge landslides. ALS differential models were the sources of new information about the dynamics of vertical displacement in the landslide and helped calculate the volume of displaced rock masses that occurred over 12 years. The cliff was found to become significantly an active in 2010. This process was observed by analysing the relief of multitemporal digital elevation models, differential models, AND morphological sections and by conducting long-term field observations. The ERT surveys made it possible to generate two 3D ERT electrical resistivity models that provided much new information about the geological structure of the cliff. Additionally, a 2D ERT profile was made through the landslide. The internal structure of the landslide was recognized, and the depth of the slip surface was estimated. The results permitted clarifying the cause of the high landslide activity and the rapid rate of retreat of the cliff edge over the past 12 years. In addition, by means of the results of electrical resistivity surveys and the use of archival boreholes, it was possible to extrapolate a model of the surface relief of the clay hill using geostatistical methods. It was found that at the boundary with the active landslide—the top of the clay layer—is tilted towards the north, i.e. towards the sea, which favours the activation of the landslide. The proposed research methodology, as well as the obtained information, may be of significant assistance in further diagnosis and prognosis of the dynamics of landslide development and the causes of landslide formation within cliff coasts.

Keywords Airborne laser scanning · Electrical resistivity tomography · Differential models · Voxel models · Landslide

Introduction

In many regions of the world, cliff coasts are the subject of comprehensive scientific research (Emery and Kuhn 1982; Hapke et al. 2009), especially in areas where progressive marine abrasion and landslide processes threaten local infrastructure and human life (Gibb 1978; Lee 2008; Bezerra et al. 2011; Hackney et al. 2013; Terefenko et al. 2018; Prémaillon et al. 2018). In Poland, the cliff coast particularly threatened by landslides is the one in the area of Jastrzębia Góra, located on the southern coast of the Baltic Sea (Fig. 1) (Subotowicz 1982, 2000, 2003, 2015; Uścinowicz et al. 2014, 2017). Dangerous landslide events continue to occur on the cliff, and the installed protective systems for prevention of both abrasion and landslides are perpetually being destroyed. The cliff is therefore at constant risk of landslide development (Subotowicz 2015).

In the cliff edge zone, local infrastructure is constantly being developed (e.g. hotels, guesthouses), which additionally weighs down the slope contributing to a loss of its stability. Moreover, the gradient of the cliff causes loss of stability and landslide formation or activation. The formation and reactivation of landslides are also favoured by the relevant geology, hydrogeological conditions, marine abrasion, and intense rainfall (Subotowicz 1982; Kramarska et al. 2011).

✉ Mirosław Kamiński
  miroslaw.kaminski@pgi.gov.pl

1 Polish Geological Institute – NRI, Rakowiecka 4,
   Warsaw 00-975, Poland

Fig. 1 Study area. **A** Location on the Landsat 7 ETM + satellite imagery. **B** Location on the orthophoto (buildings and a forest are located in the edge zone of the cliff). **C** Location on the shaded relief map
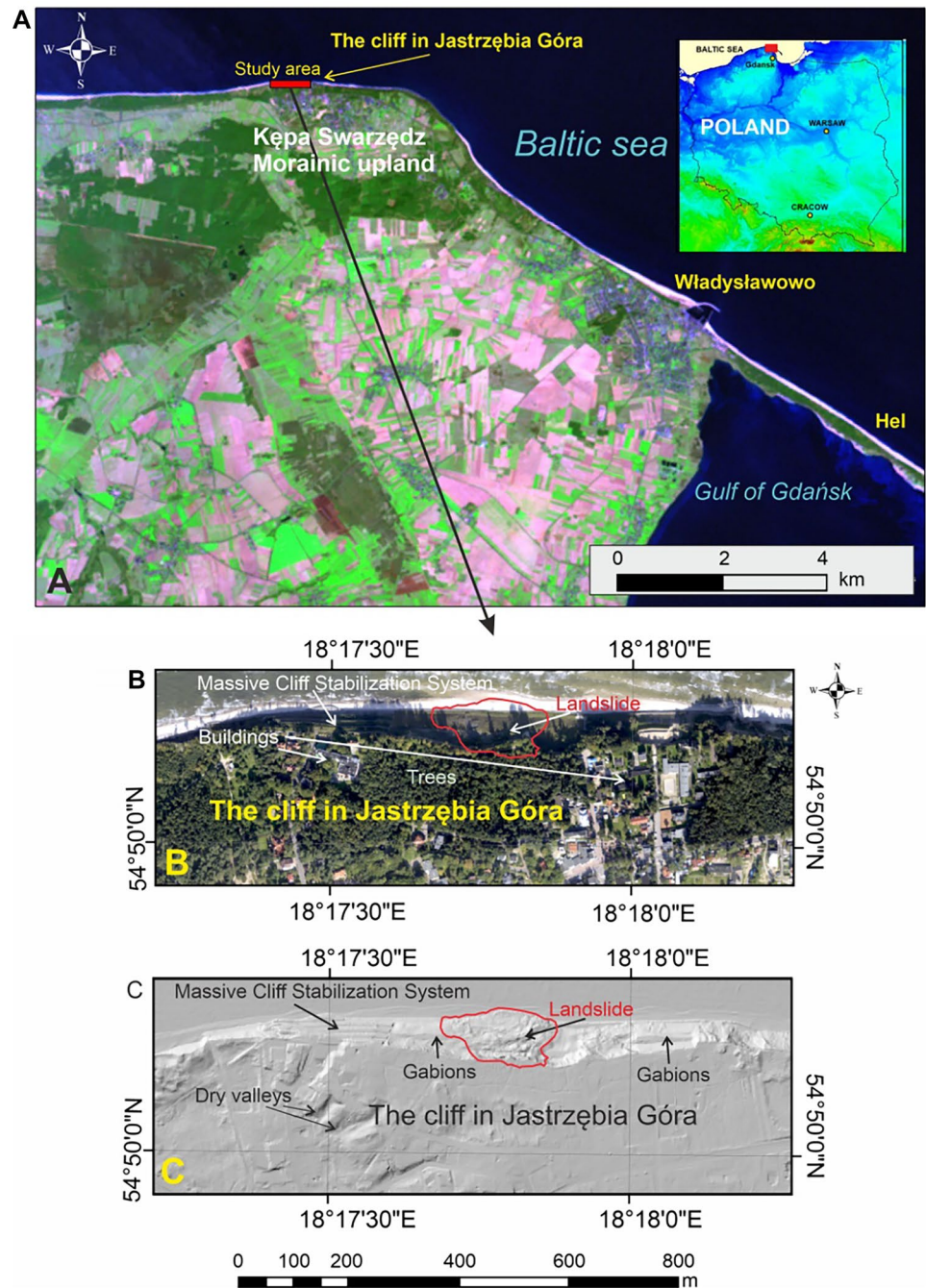
In Eastern Europe, a particular revival of mass movements was recorded after the catastrophic rainfall events of May and June 2010 (Kamiński 2011). There was then a sudden increase in the water level both in rivers and in groundwater. As a result, with the favourable geology and geomorphology, many landslides were initiated or became active in many regions of Poland, including Jastrzębia Góra. This event is known in Poland as a "landslide catastrophe" (Rączkowski 2019). In Jastrzębia Góra, landslides pose a particular threat to residential buildings, hotels, guesthouses, and other infrastructure located in the cliff edge zone. Therefore, continuous remote sensing of cliff areas and accurate spatial recognition of their geology to determine the causes of landslides is important. The methodology implemented so far to study the cliff at Jastrzębia Góra has been mainly based on photogrammetry using traditional geodetic measurements and ground photos (Subotowicz 1982, 1989, 1991, 2000; Zhang et al. 2010, 2011) or analysis of aerial and satellite images (Furmańczyk 1994). Comparative analysis of the obtained data allowed us to infer the rate of changes in the relief.

For many years, LiDAR (Light Detection And Ranging) laser scanning has been used to monitor coastal cliff dynamics. The results of laser scanning include accurate digital terrain models that enable interpretation of geomorphological structure and monitor changes in relief. Two approaches to utilizing this technology exist. The first is to perform Terrestrial Laser Scanning (TLS) in a static or mobile manner (Kramarska et al. 2011; Dewez et al. 2013). In the second, laser measurements are performed from an ALS aircraft or a UAV (unmanned aerial vehicles) drone (Young and Ashford 2006; Derron and Jaboyedoff 2010; Kramarska et al. 2011; Earlie et al. 2015). Therefore, in relation to the latest trends of researches to study the dynamics of the cliff in Jastrzębia Góra, long-term airborne laser scanning (ALS) data, publicly available on the Internet (https://www.umgdy.gov.pl), were used.

ALS data collection has been performed almost every year since 2008 upon the order of the Maritime Office in Gdynia. From these data, differential models were generated to represent the dynamics of the land surface changes and to calculate the volume of displaced rock masses that occurred between 2008 and 2020. The internal structure of landslide colluviums is usually measured by direct geotechnical investigations (i.e. borehole, in situ, and laboratory tests). Standard geotechnical investigations are essential for providing detailed information about landslide material. However, this technique cannot be used for large areas as it is expensive and labour intensive. Well-planned geotechnical borings are essential for spatial recognition of the internal structure of the slope under study. Therefore, preliminary investigations using geophysical methods are often used to plan the location of geotechnical investigations (Samodra et al. 2020). Geotechnical investigations are mainly performed in order to identify the mechanisms of the formation of a landslide and to assess the stability of the slope on the basis of geotechnical properties of the soil (e.g. plasticity index, density, bulk density, natural moisture content%, and fraction content%). It is an expensive and time-consuming examination. The ERT method is a good replacement for geotechnical research because it is cheaper and enables faster interpretation of the structure of the landslide and the geology of the cliff (Wróbel et al. 2022). Preliminary investigations using geophysical methods are often used to distribute direct geotechnical investigations (Samodra et al. 2020). In our work, in order to understand the reasons for the high dynamics of the cliff edge and the landslide surface, geophysical surveys were carried out using the ERT method. It is worth noting that the ERT method has been applied with great success for several years in the electrical resistivity study of landslides, as well as cliff coasts. Electrical resistivity tomography is one of the most common geophysical methods used for identifying geology of cliffs and studying landslides (Jongmans et al.

2000; Lapenna et al. 2003; Kamiński et al. 2012, 2014; Kamiński 2015; Perrone et al. 2014; Ling et al. 2016; Kamiński and Zientara 2017; Pazzi et al. 2019; Whiteley et al. 2019; Alpaslan and Bayram 2020).

Most commonly, ERT measurements are made in a 2D measurement system (Lapenna et al. 2003; Kamiński et al. 2014) and less frequently in a 3D measurement system (Santarato et al. 2011; Kamiński et al. 2021). In recent years, the use of the 3D ERT method for electrical resistivity testing has been gaining more popularity because it allows avoiding errors and artefacts caused by failure to meet the conditions of the 2D model. Methodologies for 2D and 3D ERT data collection and modelling are described widely in the literature (Dahlin et al. 2002; Lapenna et al. 2005; Loke 2019). The 3D ERT method allows the production of spatial or volumetric models of subsurface resistivity distributions from which features of contrasting resistivity may be located and characterized. Comprehensive integration of photogrammetric and geophysical data makes it possible, at a low cost and quite quickly, to obtain information on changes that have taken place over many years in the relief of the cliff area and to indicate the main causes of landslide movements. The aim of this research was to detect and characterize the displacement and geology of cliff and an active landslide using multitemporal ALS and ERT imaging.

Study area

Geology, geomorphology, and hydrogeology of the cliff

The study area includes part of the moraine upland of Kępa Swarzędz is located approximately 10 km west of Władysławowo (Fig. 1).

The cliff has a maximum elevation of 32 m above sea level and extends over a distance of about 1 km. The field studies of the cliff are very difficult due to the dense vegetation and gabion walls (Fig. 1B). The area of Kępa Swarzędz is transected by several dry valleys 3–7 m deep, at present, strongly anthropogenically transformed (Fig. 1B). One, with an S–N course, is located in the western part of the area of research, and its bottom is made up of dry valleys (1) (Fig. 1C). In the southwest, the valley is adjacent to an extensive depression that is filled with lake and fluvial sands (5) (Skompski 1999, 2001). In the north, the upland area is directly adjacent to the sea, separated only by a narrow sandy strip of beach (3). During times of higher water levels and storms, this strip is completely flooded by seawater which, by undercutting the cliff, is one of the reasons for

triggering landslide processes and moving colluvial sediments (2) seaward. To weaken the degradation processes, the coastal zone is continuously strengthened, the beach is reconstructed, and a part of the cliff has been built over with a gabion wall (9) (Fig. 2).

The lowest-lying sediments are the limnoglacial sediments (8) of the middle stage of the Vistula glaciation process (Skompski 1999, 2001). They are formed in the form of sandy muds and clay series (Masłowska et al. 2002). They reach a maximum thickness of 23 m, descending below beach level and are glacitectonically disrupted (Skompski 1999, 2001). These limnoglacial sediments are covered by a cluster of till (7), ranging from a few to over 20 m in thickness. In previous work, two layers of till were sectioned within the cluster (Zaleszkiewicz et al. 2000). A series of variable aged fluvioglacial sediments (6) appear within the glacial till, as well as on its surface. The sediments within the glacial till are sands, gravels, and even boulders up to 1 m in diameter (Kamiński et al. 2012) and range in thickness from 1 to about 10 m in the western part of the cliff.

The sediments lying on the surface of the glacial till are mainly differentiated sands with fine gravel and thickness ranging from 1 to 2 m. In the area of research, the whole surface of the upland is overlain by aeolian sediments (4), with layers ranging from several tens of cm to approximately 1 m. Aeolian sands developed in the form of a strip of coastal dunes, ranging in thickness from 1 to 5 m, are only found in the western part of the study area.

In the Quaternary, two levels of aquifer, intertills that are associated with sediments in Eemian interglacial and subtill, were developed. They are connected hydraulically at a depth of 20–50 m. The aquifer is formed by Quaternary sands of various granulations, which are separated from the ground surface by a layer of Vistula glaciation till. The water table is tight, locally free. It stabilizes at an ordinate of approximately 10–20 m above sea level, and in the vicinity of the seashore, it descends to approximately 0–3 m above sea level (Lidzbarski and Tarnawska 2015). Groundwater runoff takes place towards the north to the Baltic Sea. Above, in the aeration zone, perched groundwater forms an
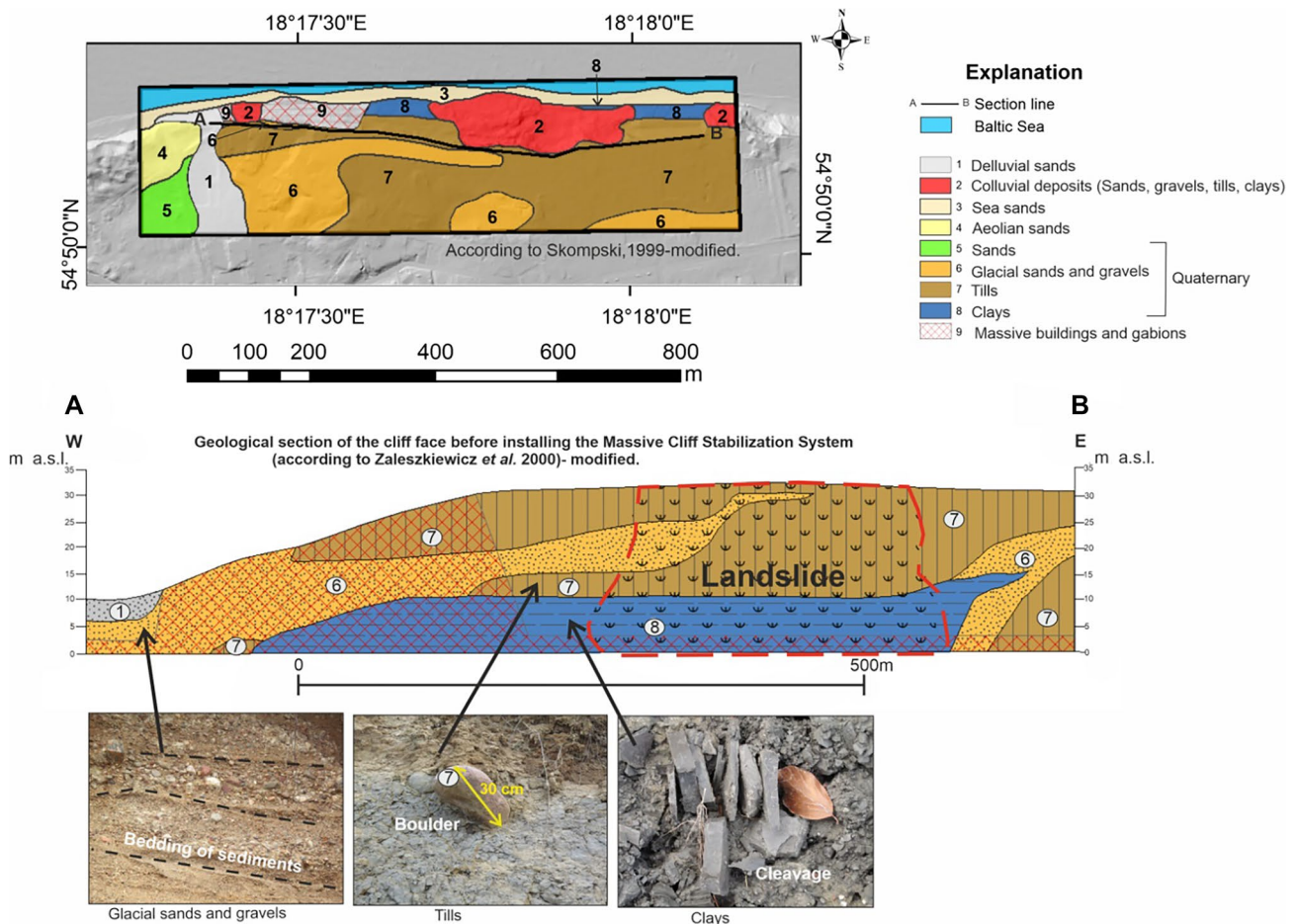

Fig. 2 Geological map of the study area against the background of the digital elevation model (according to Skompski 1999–modified). A geological section (**A–B**) and photos of rocks are presented under the geological map (clays, tills, sands, and gravels)

intermediate link in the water circulation system between the land surface and groundwater. This occurs in a wide depth range of 1–25 m and is found within sand layers in a complex of poorly permeable formations lying above the saturation zone (Lidzbarski and Tarnawska 2015).

Cliff dynamics

According to historical data, the cliff edge at Jastrzębia Góra receded by 90 m, or 1.4 m/year, between 1875 and 1937 (Majewski et al. 1983), while the average rate of cliff edge recession between 1971 and 1975 was 0.45 m/year (Subotowicz 1982, 1991, 2000). Furthermore, from 1977 to 1990, the abrasion rate was 0.9 m/year, and from 1992 to 1997, it was 1.2 m/year. The destruction caused to the infrastructure built on top of the cliff led to a decision by the Maritime Office in Gdynia to provide security measures for the shore. Between 1994 and 1997, a wall consisting of gabions was constructed along a stretch of approximately 1 km (Fig. 3A), while in 2000, a massive structure was built to protect the cliff in the area of the "Bałtyk" resort. Protection of the shore with gabion wall and massive installation did not stop the activity of mass movements, which developed surprisingly in the immediate vicinity of the massive cliff installation, on its eastern side (Kramarska et al. 2011).

Landslide

This was a rotational landslide with an irregular shape and a maximum length of about 178 m and a width of about 86 m, covering an area of about 1.4 ha (Fig. 3A). Its main body is composed of tills, clays, sands, and gravels (Kamiński and

Fig. 3 **A** Landslide visualization using LiDAR data. **B** View on the main scarp. **C** Morphology of the landslide main body. **D** and **E** View on the landslide toe
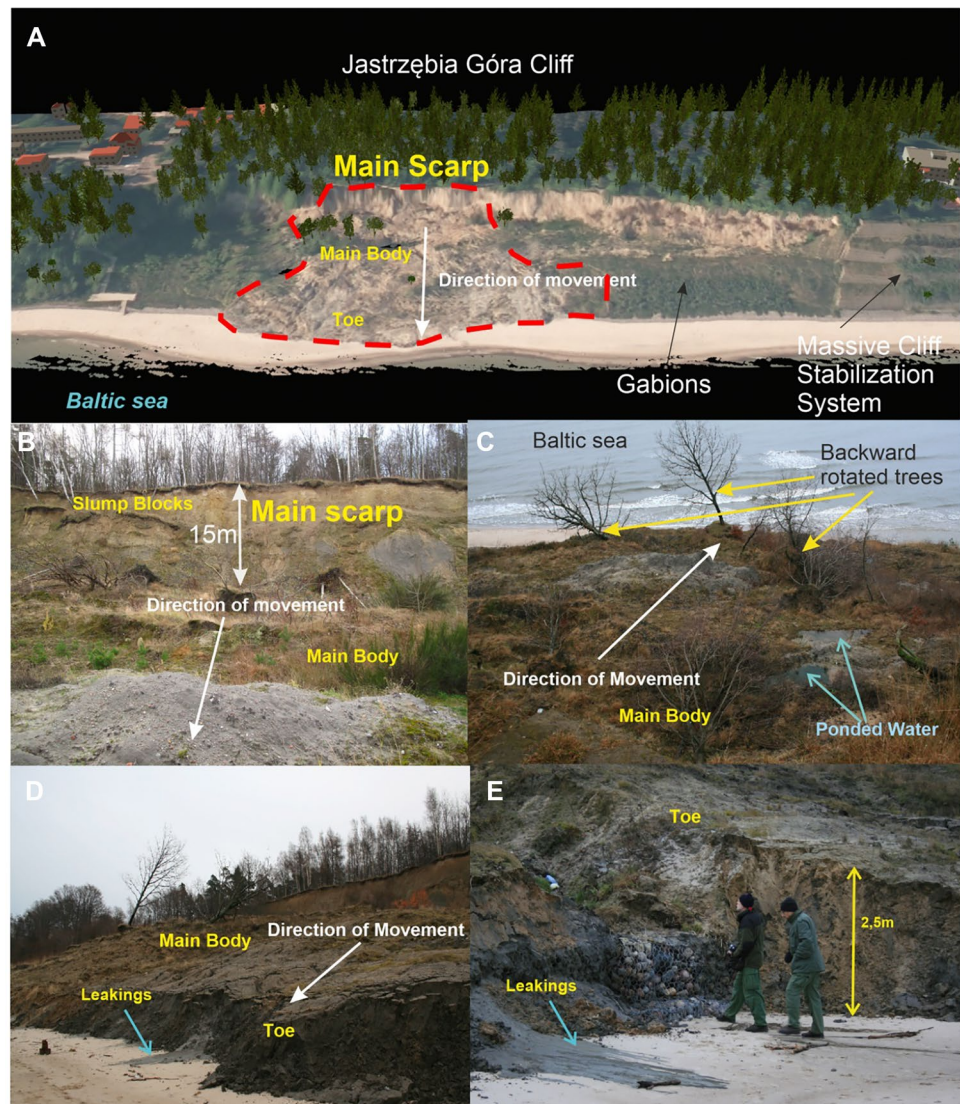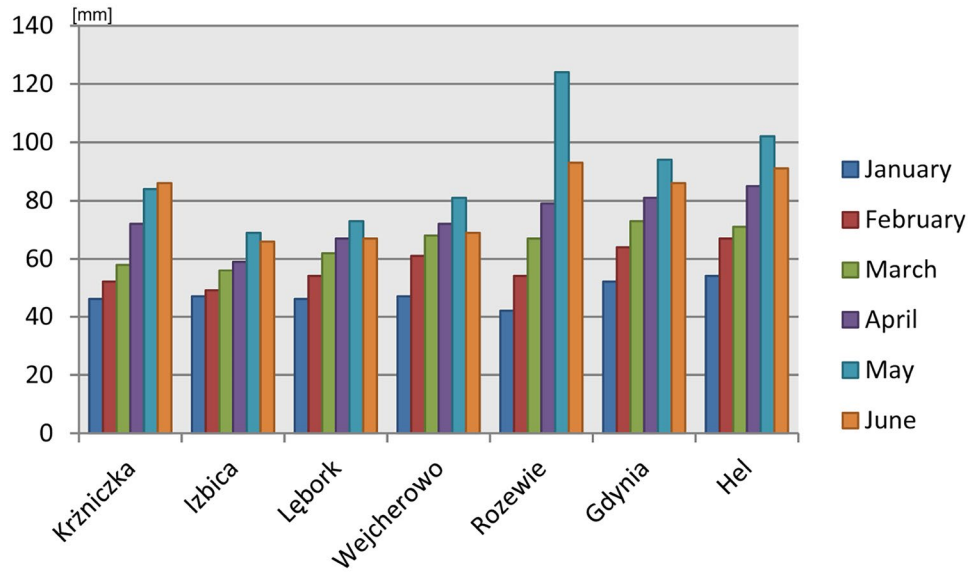
Fig. 4 Monthly rainfall graph (based on data from the Institute of Meteorology and Water Management from 2010)

Zientara 2017). The main scarp is about 15-m long, and the toe of the landslide is about 2.5-m high (Fig. 3B, E). Numerous ponded waters occur in the main body (colluvium) of the landslide (Fig. 3C).

Materials and methods

Rainfall

Meteorological data were purchased from the Institute of Meteorology and Water Management, Branch in Gdynia. Monthly rainfall totals from January to June 2010 were collected from seven meteorological stations (Fig. 4).

The highest rainfall values were recorded in May and June 2010. It was a period of catastrophic rainfall throughout Poland (Bartnik and Jokiel 2012). Also in the area of Jastrzebia Góra, there was intense and long-term rainfall. Therefore, the spatial model of monthly rainfall totals in the Jastrzębia Góra area was generated for this period. Measurement data of rainfall totals recorded by rain gauges at seven observation stations were used for modelling (Fig. 5).

Data in shape format were imported into ArcGis 10.6. Next, a cokriging algorithm was selected in the geostatistical module to interpolate precipitation values depending on the morphology of the terrain. During the modelling of the spatial distribution of rainfall amounts, a numerical terrain model is usually used as an additional variable (Hevesi et al. 1992a, b).
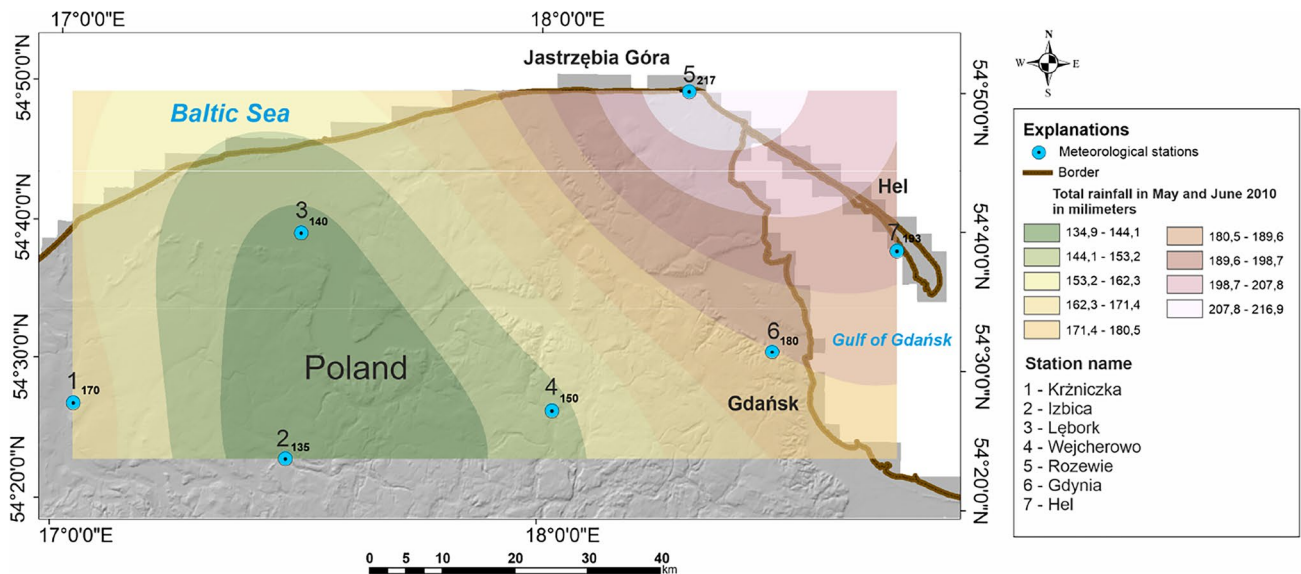

Fig. 5 Precipitation spatial model showing total rainfall in May and June 2010

Table 1 Monthly rainfall in March 2012 and April 2015—as measured at the meteorological station near Jastrzębia Góra (No.5 in Fig. 5)

Station name	Total monthly rainfall in March 2012 (mm)	Total monthly rainfall in April 2015 (mm)
Rozewie	45	34

A 2013 ALS model with a 10×10-m grid mesh was used for modelling. As a result, a model showing the spatial distribution of bimonthly rainfall in May and June 2010 was generated (Fig. 5). Because geophysical surveys were made at different times, the first measurement was made on March 28, 2012, and the second measurement was made on April 29, 2015. Therefore, the monthly sums of rainfall in March 2012 and April 2015, recorded at the meteorological station No. 5, are presented (Table 1).

Boreholes

The profiles of three archival hydrogeological boreholes (B1, B2, B4) containing information about the lithology of rocks and the height of the groundwater level (Werno 2010) and one geological-engineering borehole (B3) (Fig. 6) were employed to validate the electrical resistivity data and model the clay roof.

All information available from the boreholes was used to interpret the resistivity data in terms of the geology of the cliff. Unfortunately, in the case of B3 borehole, the data on

the geotechnical properties of the rocks was not preserved. It was thus only possible to obtain information about the lithology of rocks and the height of the groundwater table.

Electrical resistivity tomography (ERT)

Field measurements were performed using the LUND system made by ABEM, a Swedish company. The system includes a Terrameter SAS1000 single-channel electro resistivity meter, ES 10-64eC selector, multi-conductor cable sets with electrode leads every 10 and 5 m, and steel electrodes with couplings. The system was powered by a 12-V battery. The apparent resistivity data inversions were performed in Res2dinv and Res3dinv software. The used inversion method iteratively minimizes the absolute difference between the measured and calculated apparent resistivity values (L1 norm) (Loke and Lane 2002). This variant of inversion is better when subsurface structures have sharp boundaries. Maximum number of iterations was set to 5, and convergence limit for the relative change in the RMS error between 2 iterations had a default value of 5%.

The ERT method test involves recording changes in the electric field artificially created in the formation by a system of electrodes supplied with direct current (Loke 2019). The measurements are usually made along straight lines at the ground surface, and the resulting potential differences are transformed into pseudosections of apparent resistivity. Many measurement systems (electrode configurations) have
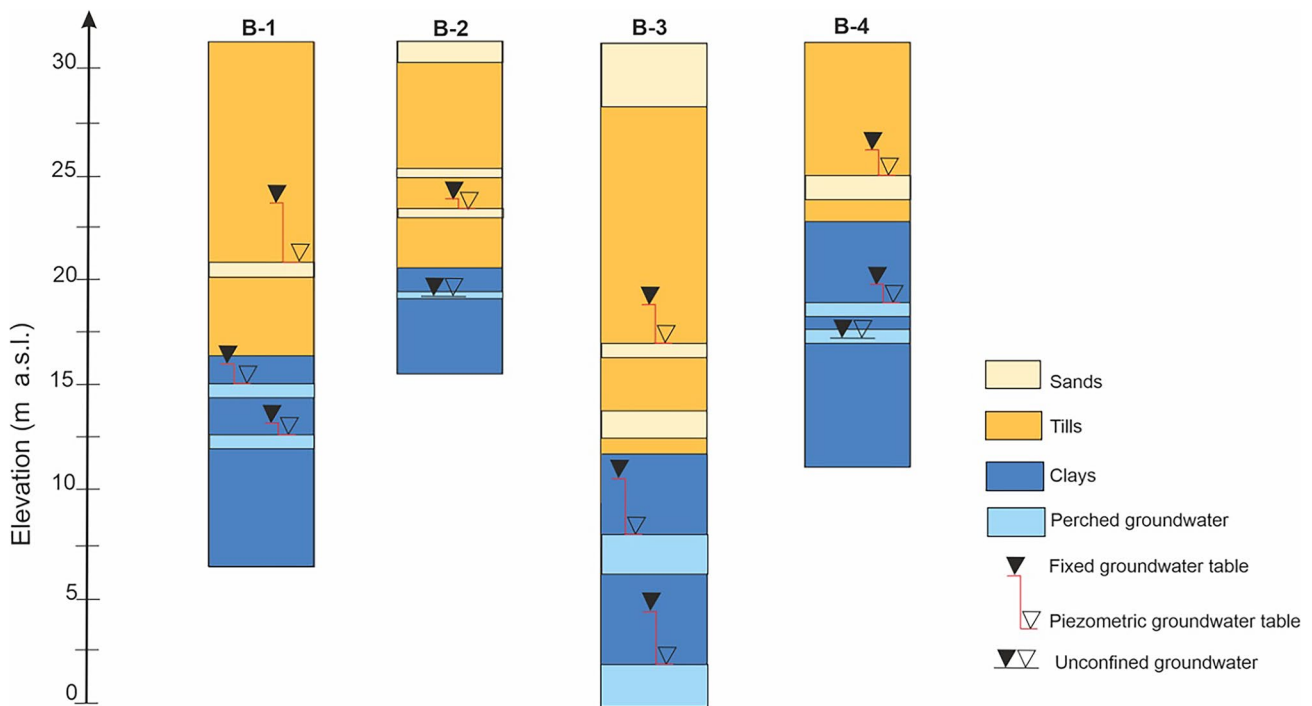

Fig. 6 Geological boreholes (Werno 2010)

been developed, e.g. Wenner, Schlumberger, dipole–dipole, and many others. The Wenner measurement system was chosen to investigate resistivity values of the cliff-building rocks due to the speed of fieldwork performed with the use of single-channel equipment (low number of measurements). Although the Wenner array is relatively sensitive to vertical changes and poor in detecting horizontal changes in resistivity (Dahlin and Zhou 2004), this array is suitable in noisy areas because of good signal strength. The field research was carried out to obtain the necessary measurement data to generate two 3D resistivity voxel models.

The first model was developed in March 2012. At that time, seven profiles of various lengths were made depending on the space availability within the site and the arrangement of buildings. The distance between the profiles was 10 m (Fig. 7). The electrodes on the profiles were spaced along a straight line every 10 m. The distance of 10 m between the profiles was chosen due to the need to generate a voxel model. According to standard procedures, separation between the lines should not be more than twice the unit electrode spacing along the lines. The depth of investigation was approximately 60 m below the ground surface to explore the largest possible area of the cliff. Profile A (38 electrodes) is the closest one to the seashore. It is located on the edge of the escarpment and has a length of 370 m. Then, at a distance of 10 m parallel to it, there is profile B (38 electrodes), also with a length of 370 m. The next profiles C, D, E, and F (39 electrodes) are each 380 m long. The seventh one, profile G (33 electrodes), is 320-m long (Fig. 7). It is

shorter than the other profiles because it could not be routed further due to fencing.

The second model was developed in April 2015. It was generated for the part of the cliff where landslide processes had developed most strongly and was undertaken so as to better understand the reason behind the high cliff activity. Four profiles with a length of 200 m were made with 41 electrode positions along each line. They were deployed on the most landslide-prone section of the scarp. The distance between the profiles was 10 m, and the electrodes were spaced every 5 m. The 5-m distance between the electrodes allowed for a more detailed resistivity image of the active part of the cliff. Profile H is located closest to the seashore; then parallel to it, at a distance of 10 m, there is profile I and then profiles J and K (Fig. 7). As a result of the inversion, the resistivity model of the data from 2012 with an absolute error of 3.99 and the resistivity model for the data from 2015 with an absolute error of 6.57 were obtained. The L profile was led by the active part of the landslides from 2015 (Fig. 7). This profile was performed using 2 m of equal 28 electrodes spacing with a total profile length of 80 m. The Wenner measurement system was also chosen to investigate resistivity values.

The 3D inversion method was applied to generate two 3D resistivity voxel models of the cliff. To obtain the 3D images, we took the 2D ERT profiles along parallel lines, combined the data into a single set, and subjected them together to 3D inversion using dedicated software, in this case, the Res3dinv software (Loke and Barker 1996;
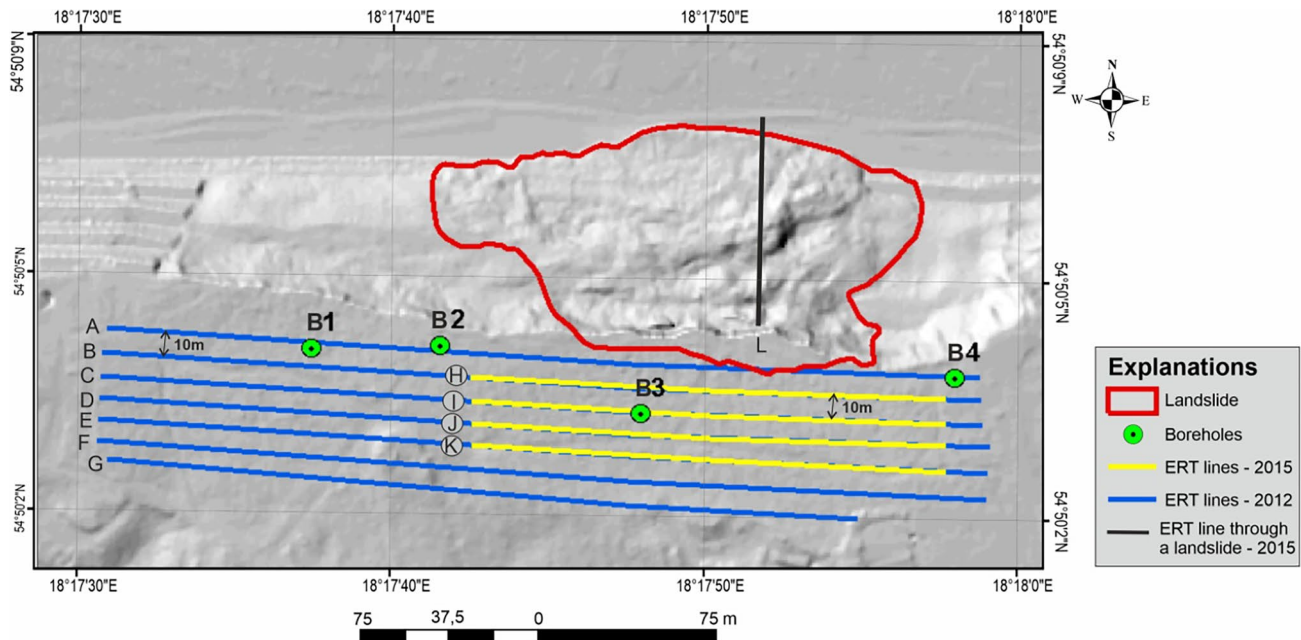

Fig. 7 Location of ERT profiles and geological boreholes

Loke 2019). The inversion routine 3D used by the program Res3dinv is based on the smoothness-constrained least-squares method (Loke et al. 2003). One advantage of this method is that the damping factor and roughness filters can be adjusted to suit different types of data. This program applies the Gauss–Newton method that recalculates the Jacobian matrix of partial derivatives after each iteration (Loke and Lane 2002). The inversion program divides the subsurface into a number of rectangular prisms and attempts to determine the resistivity values of the prisms so as to minimize the difference between the calculated and observed apparent resistivity values—subject to selected constraints (Loke 2019). The 3D inversion provided much smoother results with fewer 3D artefacts than in the 2D inversion. The 3D inversion is, however, in itself, more time and computation power consuming than 2D inversion, and considerable amounts of work hours are required to fine-tune the parameters sufficiently.

Airborne laser scanning

Multitemporal ALS data obtained with the airborne laser scanning method were used to study the cliff dynamics. This is a method that has been used for several years with great success worldwide to study the dynamics and monitoring of mass movements (Mora et al. 2003; Baldi et al. 2005; Kaminski 2011; Kamiński et al. 2021).

Airborne laser scanning (ALS) data were obtained from a map portal available on the website of the Maritime Office in Gdynia, which has commissioned airborne laser scanning of the Baltic coastal zone almost every year since 2008. The data collection (airborne survey) was conducted between 2008 and 2020 during the Spring and Autumn seasons (Table 3). The aerial LiDAR mapping was designed so that at least one flight line ran over the water, due to the need to register dunes slopes and the steep cliff face. The availability of these data is, depending on the year of execution, either in the form of a GRID structure together with measured elevation point data in LAS (Laser File Format) or the form of a GRID structure only (Table 2).

Most of the ALS data were available in a GRID structure with 1×1-m pixel resolution. Only the 2020 data were available in both LAS format and GRID structure with 0.5×0.5-m pixel resolution. In order to generate differential models, classification and filtering of the 2020 ALS point data cloud were performed. The result was a 1×1-m resolution ALS model. The point data cloud filtering and classification process were performed using dedicated QCoherent LP 360 software.

The process of generating digital ALS models is widely reported in the world literature (Axelsson 2000; Liu et al. 2005; Wang and Tseng 2010). The first step of the research was to automatically classify the point data cloud into appropriate layers. Depending on their height, the data points were classified into the following layers: "low points", "water", "ground", "low vegetation", "building", "medium vegetation", and "high vegetation". After a thorough analysis of the results of the automatic classification of ALS point clouds, different types of errors were found. These included selected parameters characteristic for the specificity of a given area, such as the following:

- To the class of points representing the ground, the points lying below the ground are included, which causes unnecessary local depressions.
- The ground class includes points representing low vegetation.
- Building walls are classified as vegetation class.
- Some roofs of buildings remain in the high vegetation class.

There are several tools in the QCoherent software to correct auto-grading errors. These are as follows:

- Correction of individual points
- Correction of points inside a circle/rectangle
- Correction of points located under or, above a given plane
- Correction of points located between two given lines

The second step in processing the classified elevation point data cloud was to filter out the "ground" points to generate a digital terrain model. A deterministic IDW (Inverse Distance Weighting) algorithm was used to geostatistically interpolate the "ground" points (Davis 2002). As a result, a GRID digital terrain model with 1×1-m resolution was generated (Fig. 8).

However, the ALS method also has limitations. The problem is, e.g. the density of scanning and the time of year of the activity. For example, the density of ALS data from 2008 was 4 p/m², while in 2020, it was 12 p/m². Moreover, the 2008 ALS data comes from the Spring (April) program, while the 2020 ALS data was obtained in the Fall (October). The density of vegetation was different in each of these periods of the year. In April 2008, it was slightly lower than in October 2020. Also, the accuracy of filtering and automatic classification of points representing the surface may have affected the final modelling effect. It is worth mentioning

Table 2 ALS data parameters

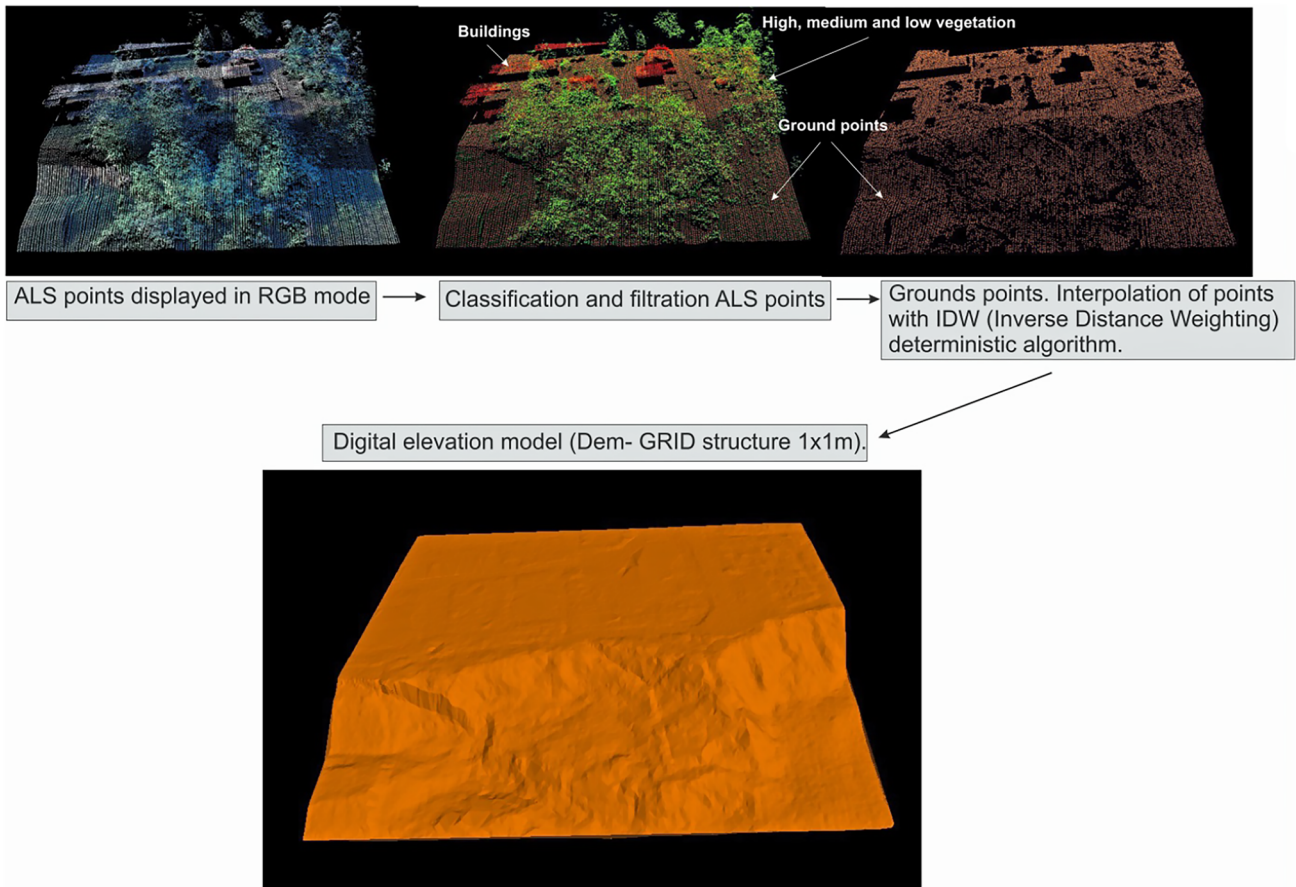| ALS data	Data of the raid by plane	GRID structure	LAS format
2008	24.09.2008	1×1 m	4p/m²
2010	10.09.2010	1×1 m	-
2012	29.09.2012	1×1 m	-
2014	22.04.2014	1×1 m	-
2020	23.03.2020	0.5×0.5 m	12p/m²

Fig. 8 Methodology of DTM generation from ALS data

that some of the ALS models were only available in the GRID structure and it was not very clear what mistakes were made in their development.

ALS results

Dynamics of the main scarp

Five digital ALS models were used to determine the landslide dynamics. With the use of analytical tools in ArcGis software, four differential GRID models were generated to represent the amount of vertical displacement within the main scarp, and four models were generated to represent the volume of displaced rock masses. Differential models

were digitally generated between the following digital ALS terrain models (Table 3).

Then, using the analytical tools available in ArcGis in the Spatial Analyst module, the values of vertical displacements of rock masses in the landslide were calculated (Table 4) and (Fig. 9).

A clear activation of the landslide was found on the differential model 2008–2010. The highest values of vertical displacement are found on the model 2008–2014, while the lowest values of vertical displacement are shown on the model 2008–2020 (Fig. 9). There are small differences in vertical displacement values between the 2008–2014 and 2008–2020 models. Using the "Cut Fill" function in the ArcGis software, it was also possible to calculate the

Table 3 ALS differential models

Number	ALS differential models
1	2008–2010
2	2008–2012
3	2008–2014
4	2008–2020

Table 4 Vertical displacements in the landslide

ALS differential models	Positive elevation [m]	Negative elevation [m]
2008–2010	5.6	12.6
2008–2012	6.3	14.4
2008–2014	5.6	18.1
2008–2020	5.5	19.7

Fig. 9 Difference between digital elevation models. The differences are shown as shaded relief—coloured reddish for the positive elevation (erosion) and bluish for the negative ones (accumulation)
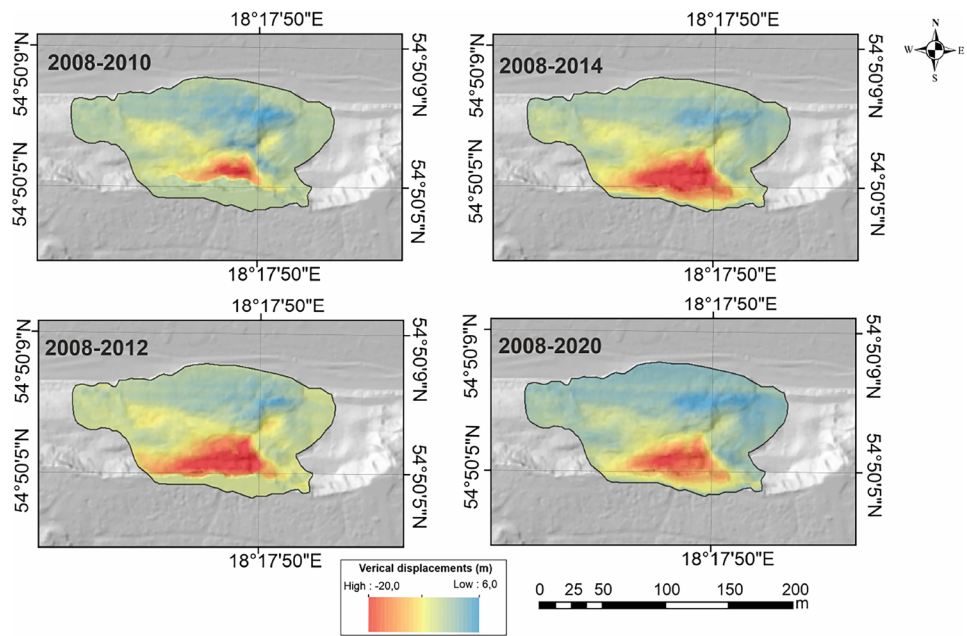
volumes of rock masses that moved during each time interval (Table 5) and (Fig. 10).

Differences between the volume of displaced rock masses and the volume of rock that has accumulated are caused by the removal and destruction of colluvium by marine abrasion in the vicinity of the toe of the landslide. The results of the differential model analysis show a clear activation of the landslide on the 2008–2010 model. In contrast, there are small differences in the volumes of displaced rock masses between the 2008–2014 and 2008–2020 models. Studying the course of the morphological lines (2008, 2010, 2012), it was found that in 2010, the landslide became active. Between 2008 and 2010, the edge of the cliff has moved backward about 11 m. The sudden activation of the landslide should be associated with the intense rainfall that occurred in May and June 2010 (Fig. 5). During this time, groundwater levels rose in many regions of Poland, including Jastrzebia Góra (Rączkowski 2019). Between 2010 and 2012, the edge of the cliff has moved backward 7 m and between 2012 and 2014 already 13 m. After 2014, we observe a calming of landslide movements; as between 2014 and 2020, the edge of the cliff has moved backward only 2 m (Fig. 11). A morphological section made between the 2008 2010, 2012, 2014, and 2020

Table 5 Volumes from accumulated and eroded rock masses

ALS differential models	Net gain [m^3]	Net loss [m^3]
2008–2010	11,082	13,361
2008–2012	15,207	23,468
2008–2014	16,500	37,385
2008–2020	17,162	39,149

ALS models show that the cliff edge has moved backward a maximum of about 32 m over 12 years (Fig. 11).

ERT results from 2012

3D ERT profiles

Six 3D ERT sections were generated: A–B, B–C, C–D, D–E, E–F, and F–G. In all electrical resistivity profiles, the low-resistivity part (dark blue colour) with resistivity values below 30 Ω m can be distinguished. These resistivity values were attributed to clays and perched groundwater. In turn, resistivity values occurring between 30 Ω m and 90 Ω m were assigned to clays and tills, while resistivity occurring between 90 Ω m and 400 Ω m (green) were assigned to tills. The highest resistivity values above 400 Ω m were attributed to sands and gravels (Table 6).

Four borings B1, B2, B3, and B4 were used to calibrate the resistivity profiles. Two distinct boundaries were distinguished by two dashed lines in all seven 400-m long and 70-m deep soil penetration electrical resistivity profiles (Fig. 12). The first boundary clearly separates the high-resistivity rocks (green, yellow, and red) from the blue, low-resistivity clays and perched groundwater. This boundary is irregular as there are numerous glacitectonic deformations in some places (Fig. 12). These were evident on all the 3D ERT profiles. The second isolated boundary occurs at a depth of approximately 40 m below the ground surface. These are clays and perched groundwater. It was not possible to separate clays from perched groundwater. The reason was too low resolution of the model. The figures show model sections approximately at the ERT line positions (Fig. 12).

Fig. 10 Differences in volumes of displaced rock masses
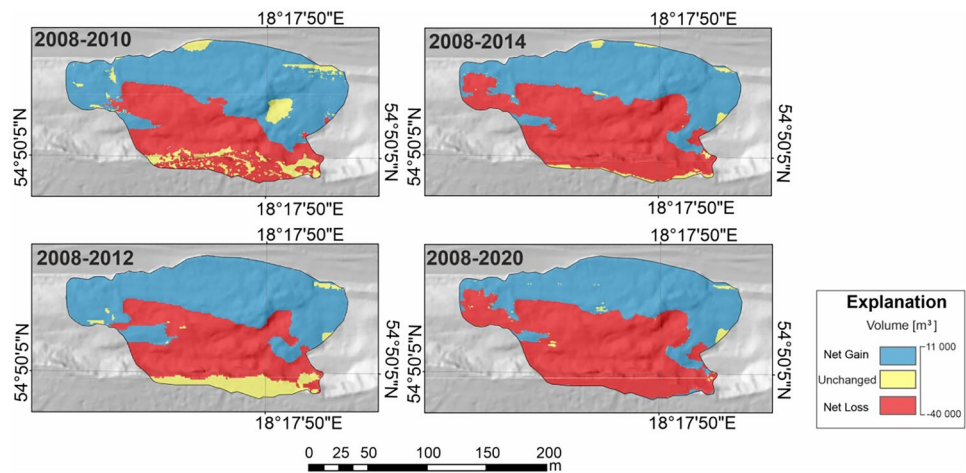
Slice map

Two irregular regions with high resistivity values (red and yellow) above 400 Ω m were marked on the 0–3-m slice map. In between are tills with resistivity ranging from 90 Ω m to 400 Ω m (green). On the southern side, at a depth of 3–6 m, the two high resistivity areas (red and yellow) merge with each other, and tills (green) are present in between. A similar resistivity distribution is seen at the 6–9-m depth (Fig. 13). A fundamental change in the resistivity distribution is seen at a depth of 9–12 m. High resistivity areas almost disappear. Resistivity values characteristic of sands and gravels are visible in a narrow yellow strip only on the southern side. The main lithological complexes are tills (green) and clays and perched groundwater (blue). At a depth of 12–15 m, only one area of tills remains visible (at a 260 m model length). At a depth of 15–18 m, only low resistivity formations (below 90 Ω m), i.e. clays and perched groundwater, occur (Fig. 13).

The voxel model

The first model was 400-m long, 50-m wide, and 60-m deep. In the generated resistivity model, two areas marked in yellow and red with resistivity above 400 Ω m became visible (Fig. 14A, B). This value was assigned to sands,

Table 6 The resistivity ranges correlated with the lithology's of the area

Resistivity in Ohm m	Lithology
< 30	Perched groundwater, clays:- unseparated
30–90	Clays, tills: unseparated
90–400	Tills, sands: unseparated
> 400	Sands, gravels: unseparated

and gravels that directly overlie the tills (green). The tills have resistivity values ranging from 90 Ω m to 400 Ω m (Fig. 14A, B).

Beneath them, there are low resistivity formations with resistivity values below 90 Ω m. These include clays and perched groundwater. The modelling of three isosurfaces was also performed for resistivity values of 600 Ω m, 300 Ω m, and 90 Ω m (Fig. 14C, D). The models of these surfaces represented the three-dimensional extent of the different roofs of the lithological complexes: sands and gravels, clays, and tills. The modelled surface of the top of clay (90 Ω m) showed considerable morphological variation, which indicates the existence of glacitectonic deformations in it (Fig. 14C).

ERT model from 2015

3D ERT profiles

Three 3D ERT sections were generated: H–I, I–J, and J–K. One boring, B3 was used to calibrate four 200-m long I–J profiles penetrating approximately 30 m into the ground. In these profiles, only one boundary separating high resistive rocks (sands, gravels, and tills) from low resistive clays and perched groundwater was distinguished (Fig. 15). Both sands and gravels occur in several patches overlying tills. This is particularly well visible on profiles H, I, and J. However, on profile K, sands and gravels form one large patch lying on tills. The figures show model sections approximately at the ERT line positions (Fig. 15).

Slice maps

Two irregular high resistivity areas above 400 Ω m were marked in red and yellow on the 0–3-m slice map. These are sands and gravels. The rest are green tills with resistivity ranging from 90 to 400 Ω m.
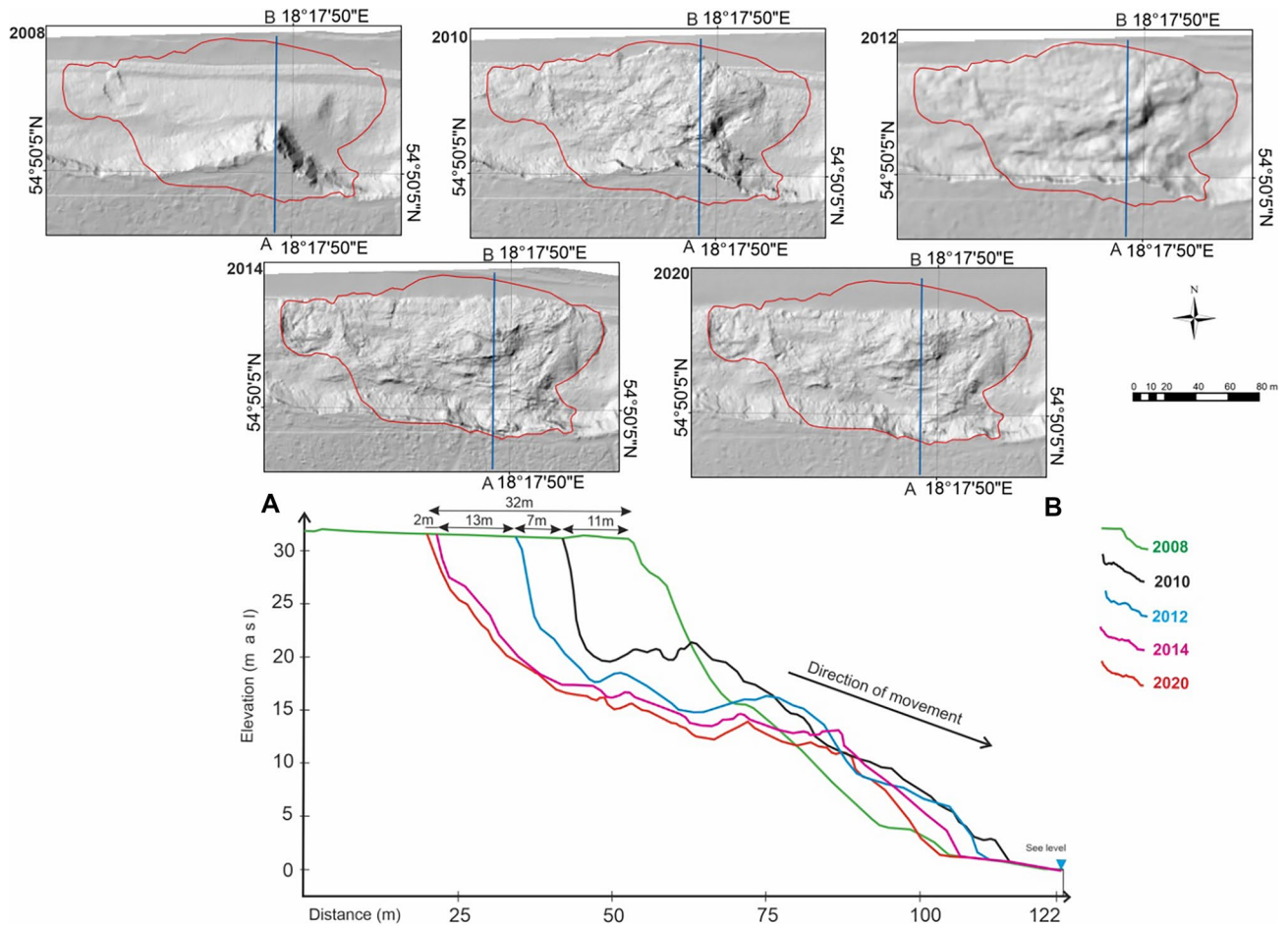
Fig. 11 **A–B** morphological sections through multitemporal digital elevation models (2008, 2010, 2012, 2014, and 2020)

At a depth of 3–6 m, both high resistivity areas (red and yellow) occur on opposite sides of the shear surface, and tills (green) occur between them (Fig. 16). The two high resistivity areas merge at a depth of 6–9 m, and only on the northern side, a small tills area is visible (green). At a depth of 9–12 m between the 50 m and 170 m model length, there is one large high resistivity area wrapped on both sides by tills. In contrast a depth of 12–15 m, the area of sands and gravels ascends only between 90 and 130 m of the model length and disappears completely at the depth of 15–18 m (Fig. 16).

The voxel model

The second model was 200-m long, 30-m wide, and 30-m deep. This model was generated for the most active portion of the cliff..In this model, only one high resistivity area (in yellow and red) (sands and gravels) with resistivity above 400 Ω m became visible (Fig. 17A, B).

Underneath these are tills (green colour). The tills have resistivity values ranging from 90 to 400 Ω m. Below the tills, there are low resistivity formations (clays, perched groundwater) with resistivity values below 90 Ω m. The modelling of three isosurfaces was also performed for resistivity values of 600 Ω m (sands and gravels), 300 Ω m (tills), and 90 Ω m (clays) (Fig. 17C). All three isosurfaces represented modelled extents of the top of bed surfaces of individual lithologic outcrops, namely, sands and gravels, tills, and clays. They have different shapes and extents (Fig. 17C, D). The isosurface (blue colour) of the top of clay with resistivity values of 90 Ω m has the most complex shape. Its undulating surface is caused by glacitectonic deformations, and at the same time, it shows a slight slope towards the north.

The difference between 2012 and 2015 ERT voxel models

It was not possible to generate a differential model because the two voxel ERT models have different resolutions and sizes. A different solution was proposed to compare the

Fig. 12 Geological interpretation of the 3D ERT sections
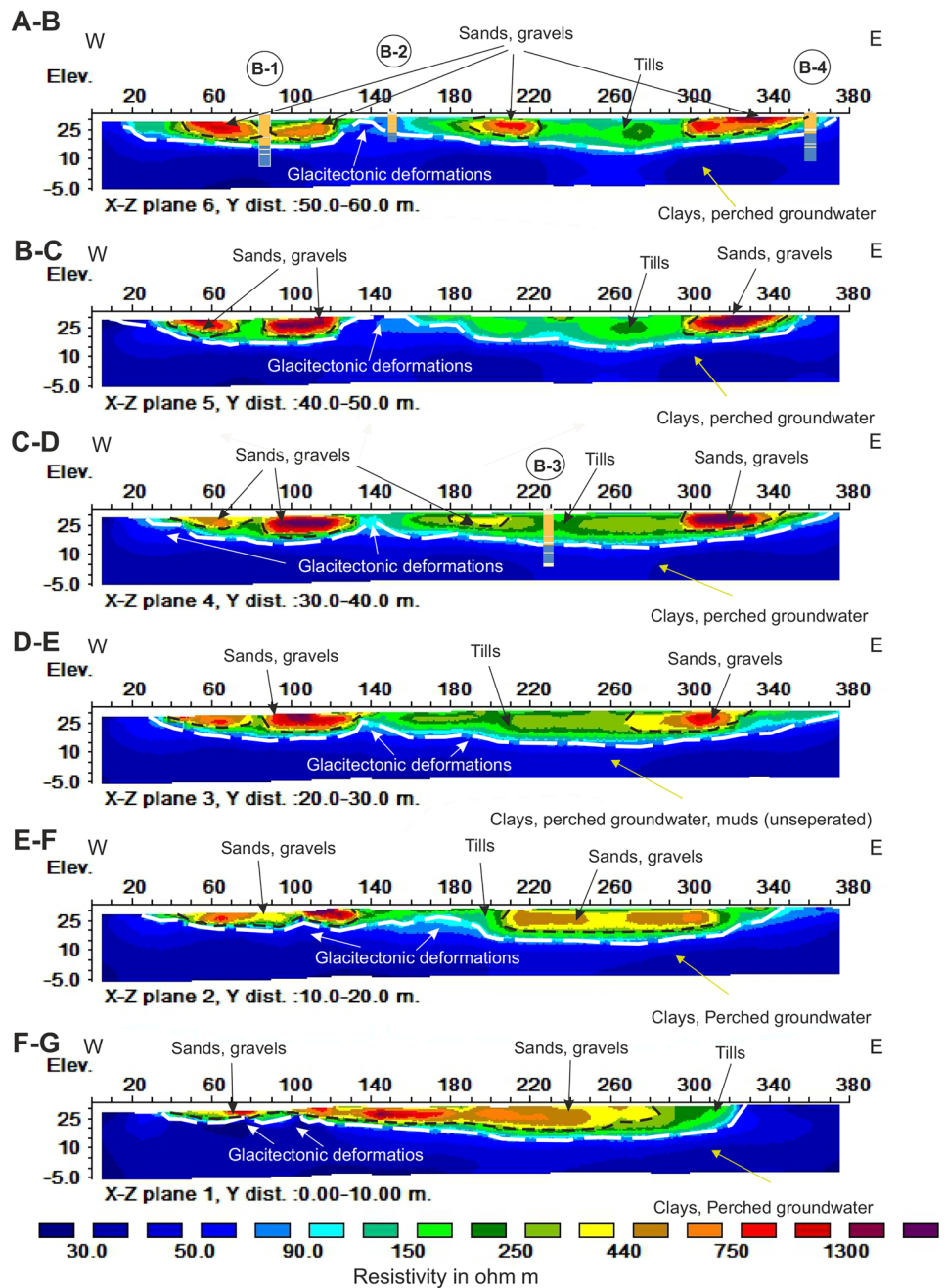

distribution of resistivity values in the two models. Well, cross-plots of the distribution of resistivity versus length were generated for each of the ERT voxel models (Fig. 18A, B). Resistivity values above 500 Ω m were the best for visual interpretation. Therefore, these boundaries on both cross-plots are marked with a black dashed line.

In the 2012 cross-plot (Fig. 18A), from 150 to 300 m, the beginning of the 2015 cross-plot is marked. In both cross plots (Fig. 18A, B), two areas (I and II) showing the

distribution of resistivity of the rock as a function of model length are marked simultaneously. It is noted that there are more voxels with values above 500 ohms in the 2015 cross-plot than in the 2012 cross-plot. Furthermore, the marked voxels (I and II) in the 2015 cross plot have a different spatial distribution than the voxels marked in the 2012 cross plot. This is particularly evident between lengths 140 m and 180 m (2015 cross-plot) and 290 m and 350 m (2012 cross-plot). These results indicate that the rocks from the 2015

Fig. 13 Slice maps at different elevations and their geological interpretation (0–3 m, 3–6 m, 6–9 m, 9–12 m, 12–15 m, 15–18 m)
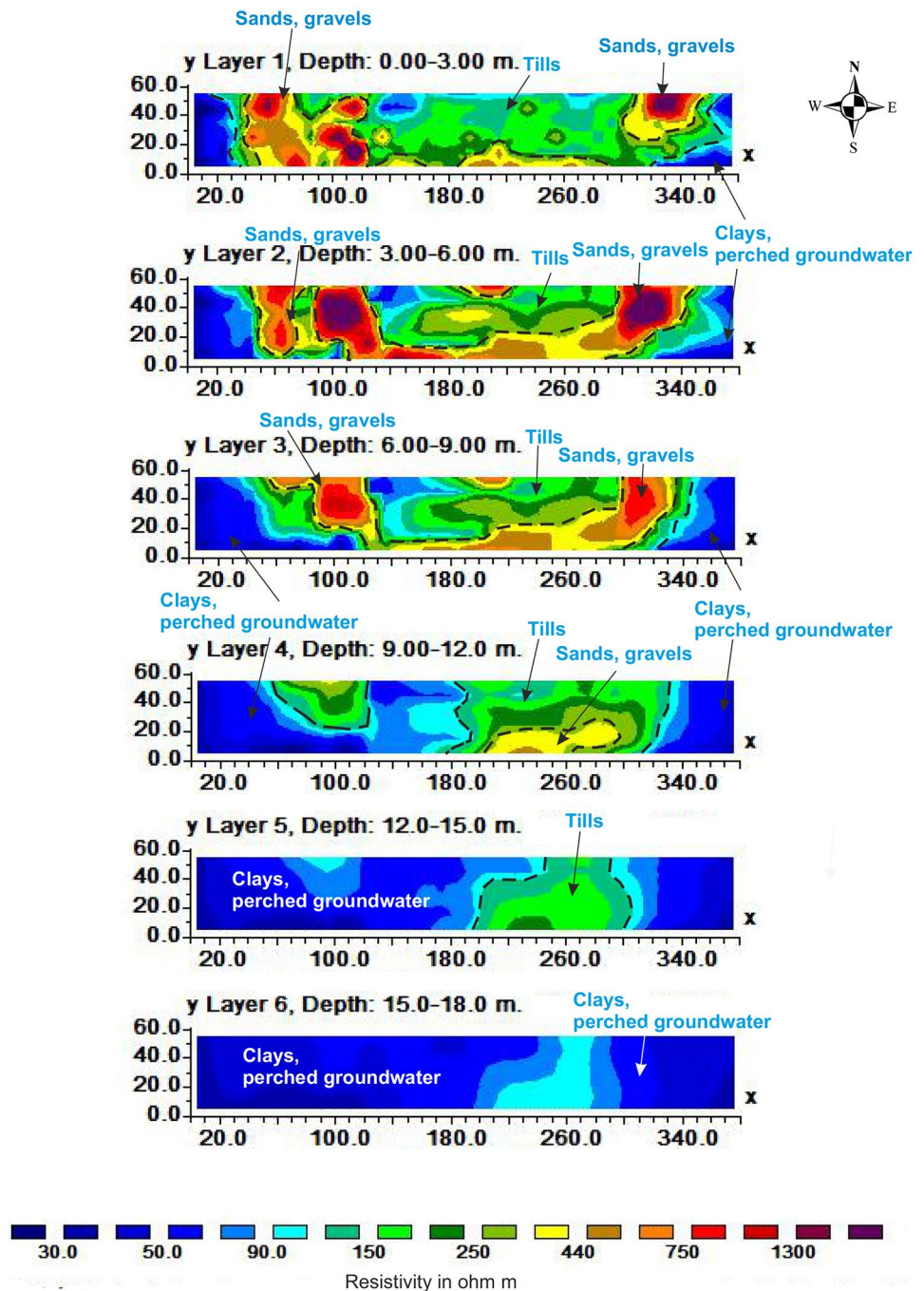
ERT model have a lower degree of water saturation than the rocks of the 2012 ERT model.

2D ERT profile (L)

The landslide main body is built of mixed tills, clays, sand, and gravels (from 10 to above 500 Ω m). There are numerous small cracks on the surface of the landslide. On the ERT profile, they have a value above 900 Ω m.

This indicates that the landslide is active. The slip surface occurs here about 8 m below the ground surface (Fig. 19). It occurs between high-resistivity (above 70 Ω m) rocks that build the main body and low-resistivity rocks with values below 40 Ω m (blue).

Under the slip surface, the occurrence of clays and perched groundwater (10–40 Ω m) was interpreted. Flow of the groundwater also occurs in the slip surface.

There are numerous leakings on the beach in the toe area.

Fig. 14 **A–B** The voxel model and vertical sections. The model showed three-dimensional distribution of resistivity. **C** Iso-surfaces for the resistivity value 90 Ω m, 300 Ω m, and 600 Ω m of electrical resistivity extracted from 3D ERT model
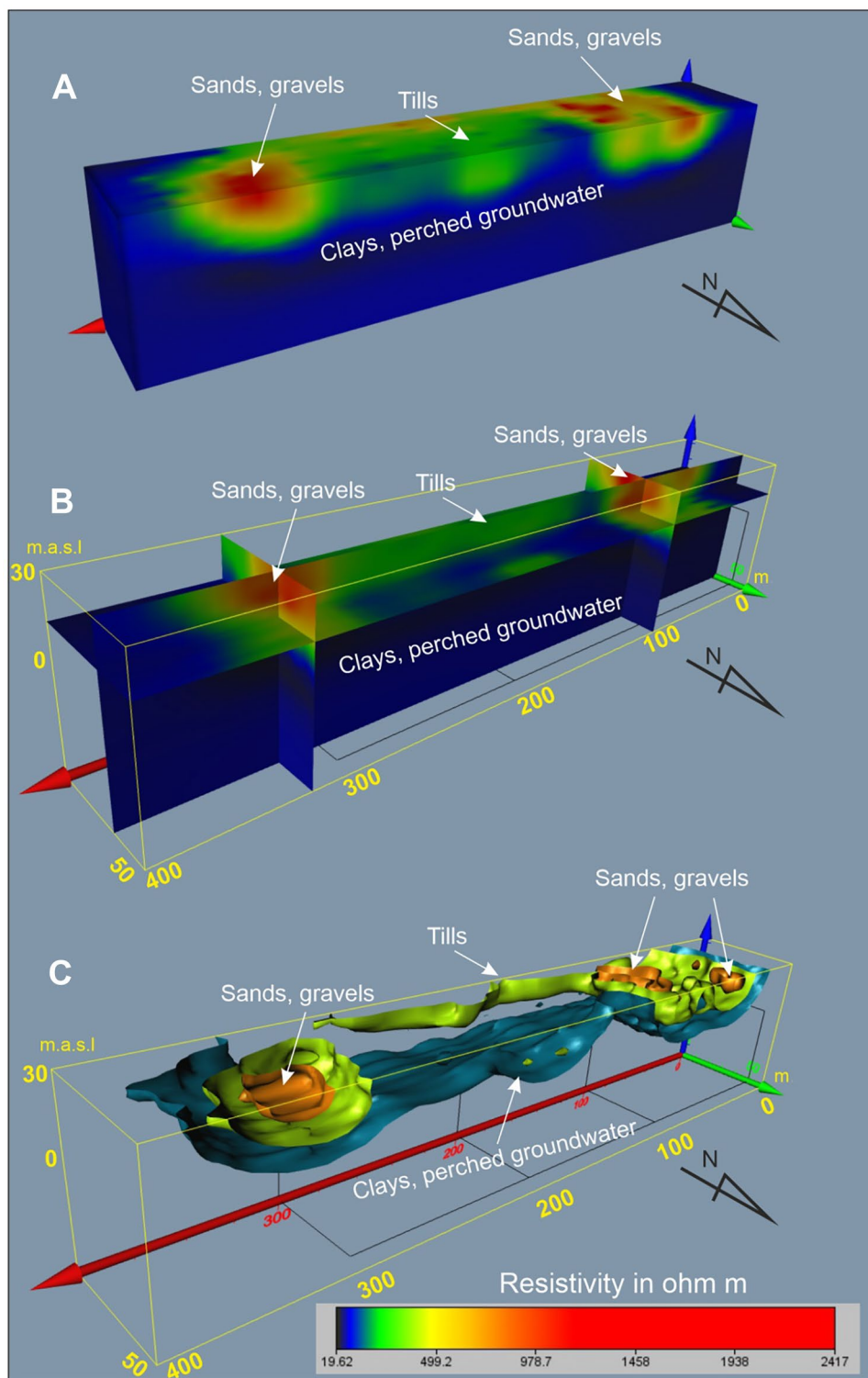

The top of clay bed surface relief model

By applying a geological interpretation of the 3D ERT electrical resistivity sections, isosurfaces (extracted from 3D ERT model 2012) and data from geological borings B1, B2, B3, and B4, a model of the top of clay bed was developed via the application of geostatistical methods. The calculated depth values were imported into ArcGis and then further modelled in the geostatistical module. A Bayesian kriging algorithm was used to interpolate the data. As a result, a model of the top of clay bed in GRID structure and pixel size of 1×1 m was obtained (Fig. 20A).

Fig. 15 Geological interpretation of the 3D ERT sections
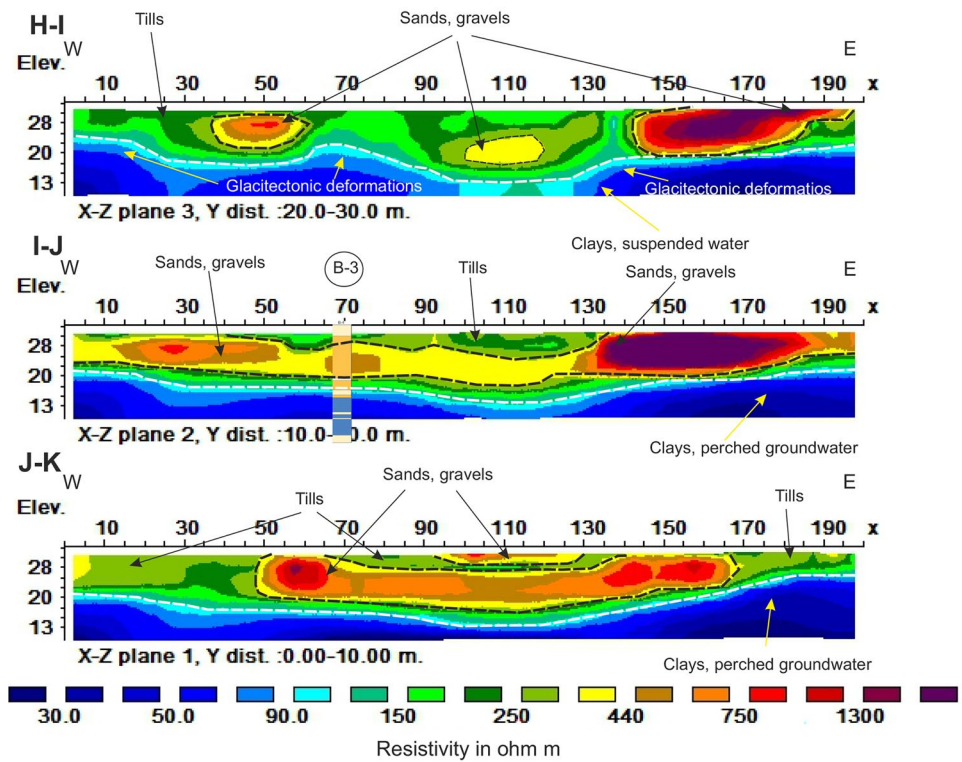
The generated model revealed that the relief of the clay bed top is strongly differentiated (Fig. 20A). In the northern part of the model, there are two areas (M and N) that are characterized by low elevation value. In the first area, M (inactive landslide), the height values range from 14.2 to 26 m (11.8 m). The second (N) is located near the B3 borehole (active landslide). The values of the height of the top of clay bed here range from 14.8 to 25.5 m (10.7 m) (Fig. 20A, B). Large differences in surface heights indicate significant glacitectonic deformations (Fig. 19B, sections A–B). In the area of the active landslide, the top of the clay bed surface is most inclined toward the north (Fig. 20B, section C). The southern part of the model is less morphologically differentiated (Fig. 20C).

Discussion

Multitemporal ALS data obtained via the airborne laser scanning method were used to study the cliff dynamics. This is a method that has been employed for several years with great success worldwide to study the dynamics and monitoring of mass movements (Mora et al. 2003; Baldo et al. 2008; Kamiński 2011; Kamiński et al. 2021). In the case of studying the dynamics of the landslide an active cliff in Jastrzębia Góra, multitemporal ALS data were used for the first time to generate differential models. This provided rapid and inexpensive spatial information on the

rate of cliff edge recession over the past 12 years and on the dynamics of changes happening in the active landslide surface, as well as the volumes of displaced rock masses. The results obtained are an excellent complement to the studies conducted by terrestrial laser scanning (TLS) (Kramarska et al. 2011). The conducted research shows that the activity of the cliff and landslides increased significantly after 2010. This can be explained by the significant spring rainfall of 2010 and, as a result, an increase in the level of groundwater.

In order to better understand the reasons for the high dynamics of the cliff edge and the landslide surface, geophysical surveys were carried out using the ERT method. By applying ERT research and the generated voxel models, it was possible to generate a new image of the geophysics of the cliff. It is worth noting that the resistivity distribution in the two ERT models is not similar to each other. This difference is particularly evident in the resistivity distribution in the cross plots (Fig. 18). After analysing the resistivity values in both cross-plots, it was found that the highest number of high-resistivity voxels (above 500 Ω m) is found in the 2015 ERT model than in the 2012 ERT model. This result is justified by the value of the monthly rainfall totals that occurred between March 2012 (45 mm) and April 2015 (34 mm). It is also worth mentioning that and analysis of morphological cross-sections by multitemporal models showed a calming of landslide movements. The cliff edge only retreated by 2 m between 2014 and 2020.

Fig. 16 Slice maps at different elevations and their geological interpretation (0–3 m, 6–9 m, 9–12 m, 12–15 m, 15–18 m)
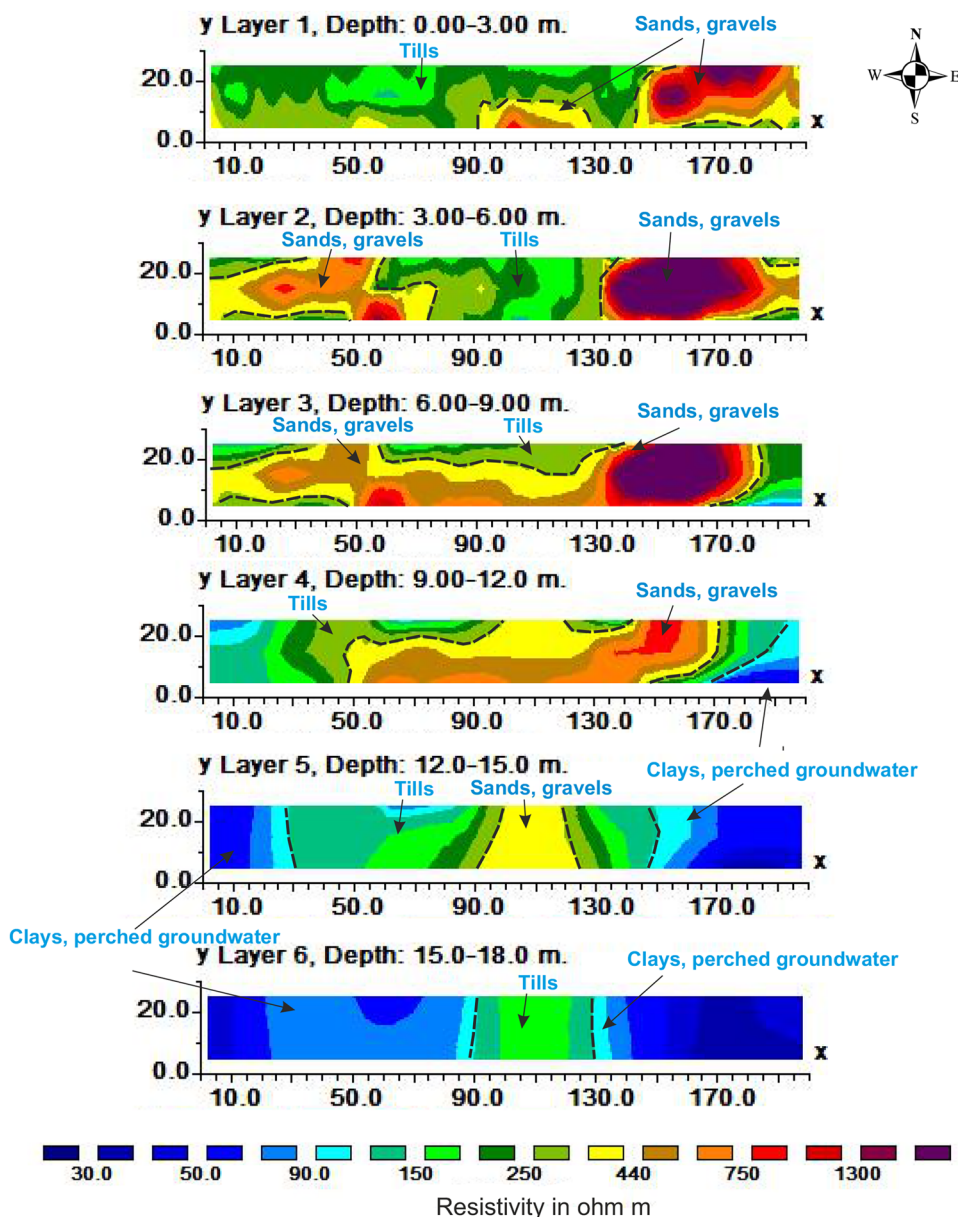

Derivative images produced from voxel models such as slice maps, isosurfaces, and vertical sections depicted the spatial distribution of rock resistivity. Based on the analysis of changes in the distribution of resistivity, the occurrence of glacitectonic deformations in the rocks forming the cliff was interpreted. Recognition of the distribution of glacitectonic deformations is important for forecasting the occurrence of further landslide movements (Overgaard and Jakobsen 2001; Jacobsen and Overgaard 2002). In our work, it was possible to interpret glacitectonic deformations on both the 2012 and 2015 voxel models. A less accurate 3D ERT model from 2012 was used for the initial interpretation of the geological structure of the cliff. On the slice map (0–3 m), the eastern part has a large area of high-resistivity sands and gravels (< 400 Ω m) adjacent to the tills. This is the most active

part of the cliff—where there is also the active landslide. The A–B geophysical cross-section clearly shows that the sands and gravels superposed on the tills and that there are low-resistivity clays underneath them.

The second 3D ERT model from 2015 is more accurate and has better resolution. This allowed us to generate a more detailed picture of the rock distribution in the most active part of the cliff. In the vertical section, from the top, we can see heavy tills superposed on the sand and gravel, which, in turn, is superposed on the clays. Such a ground arrangement becomes unstable with a certain slope and the share of groundwater. Underground waters circulating in the sand and gravel beds and on the border with the clay reduce the cohesiveness of loose rocks and increase the plasticity of the clays. Such conditions, combined with marine erosion destabilizing

Fig. 17 **A–B** The voxel model and vertical cross sections. The model showed a three-dimensional distribution of resistivity. **C** Isosurfaces for the resistivity value 90 Ω m, 300 Ω m, and 600 Ω m of electrical resistivity extracted from the 3D ERT model
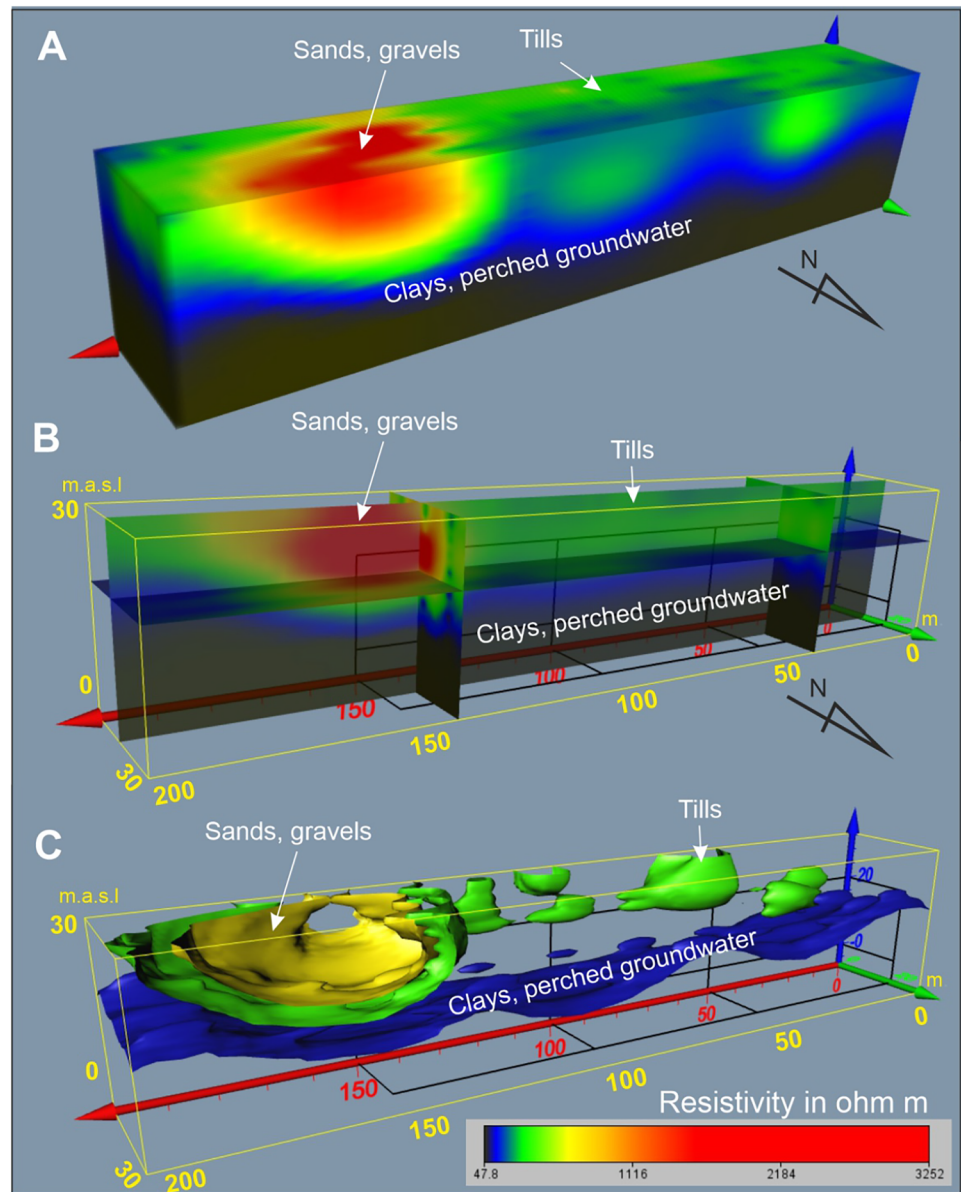
the foot of the cliff (Udphuay et al. 2011), led to the development of the landslide proper that covers the whole slope (Uścinowicz et al. 2017).

The geophysical survey of the landslide has also yielded a lot of new information. The most important was to recognize the structure of the landslide, interpret the slip surface, and present the direction of groundwater runoff. The slip surface has been interpreted between resistivity of 40 Ω m and resistivity above 70 Ω m. This sudden change in resistivity value may indicate the presence of a slip surface. In the lower part of the landslide, the maximum extent of the slip surface was determined to sea level. Also, the use of terrain morphology helped in the determination of minor scarps.

Our research also did not confirm the hypothesis that the view was expressed that the maximum slip surface may be below sea level (Uścinowicz et al. 2014). The image of the

landslide structure presented in archival geotechnical studies (Werno 2010) was significantly simplified compared to the results of our research. The results of the ERT and ALS studies indicate that the studied landslide should be classified as a rotational landslide. This is indicated by the results of the geological interpretation of the ERT profile (L) and the morphology of the landslide surface. This is particularly well shown on the morphological cross-sections by the multitemporal models (Fig. 11).

An important problem was the development of the top of clay bed surface relief model. Generating the isosurface (600 Ω m) of the top of the clay bed was key to the development of the spatial model.

When analysing the top of clay bed model, it was found in the northern part of the model, two areas (M and N) have low elevation values. Despite the similar height values

Fig. 18 The cross-plots of rock resistivity distribution along the length of the models from 2012 and 2015. Two the areas (I and II) with rock resistivity values above 500 Ω m were distinguished on both cross-plots. **A** Visualisation of the distribution of rock resistivity as a function of ERT length—2012 ERT voxel model. The range of the 2015 ERT model is marked between 150 m in length and 350 m in length. **B** Visualisation of the distribution of rock resistivity as a function of the length—2015 ERT voxel model
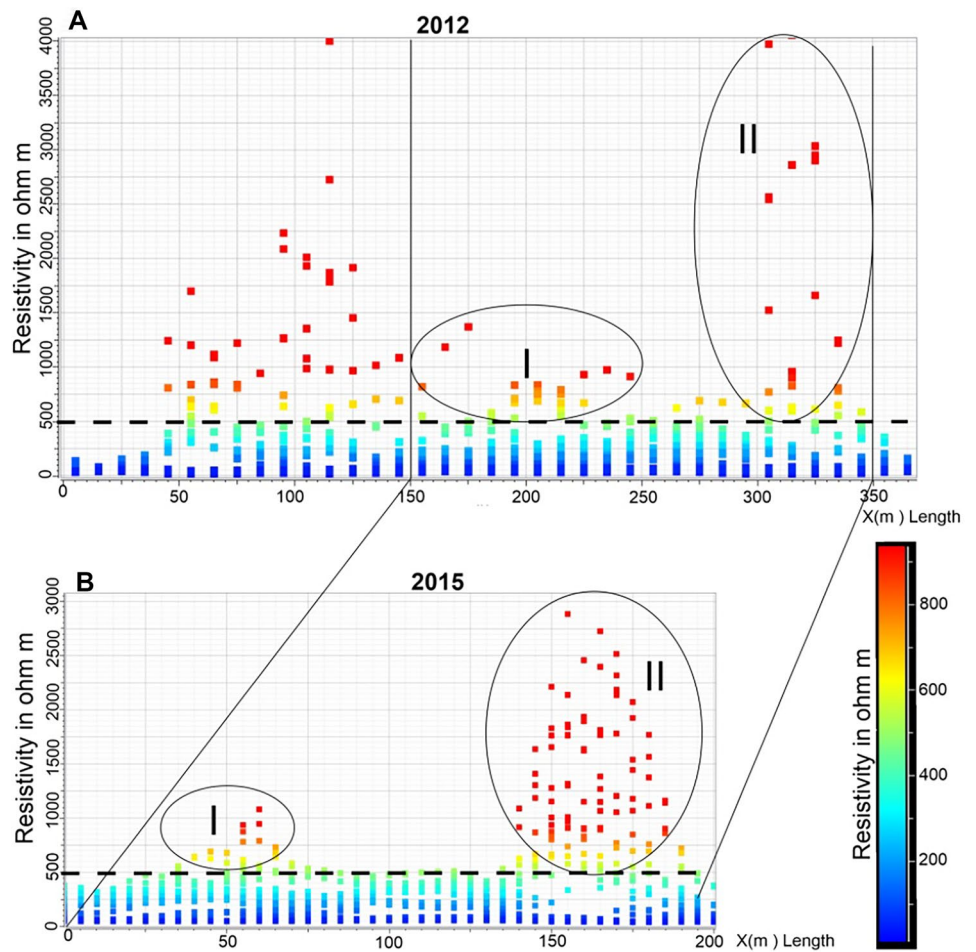
of the top of bed, only the landslide in the area of the B3 borehole (N-area) is active. In contrast, near borehole no. 1 (M-area), the cliff-face is currently inactive. In the past, the entire area of the cliff was built up and stabilized by the placement of special engineering structures called gabions (Subotowicz 1991). Unfortunately, in 2010, as a result of the sudden activation of the landslide, most of the gabion wall was completely destroyed. However, in the inactive areas of
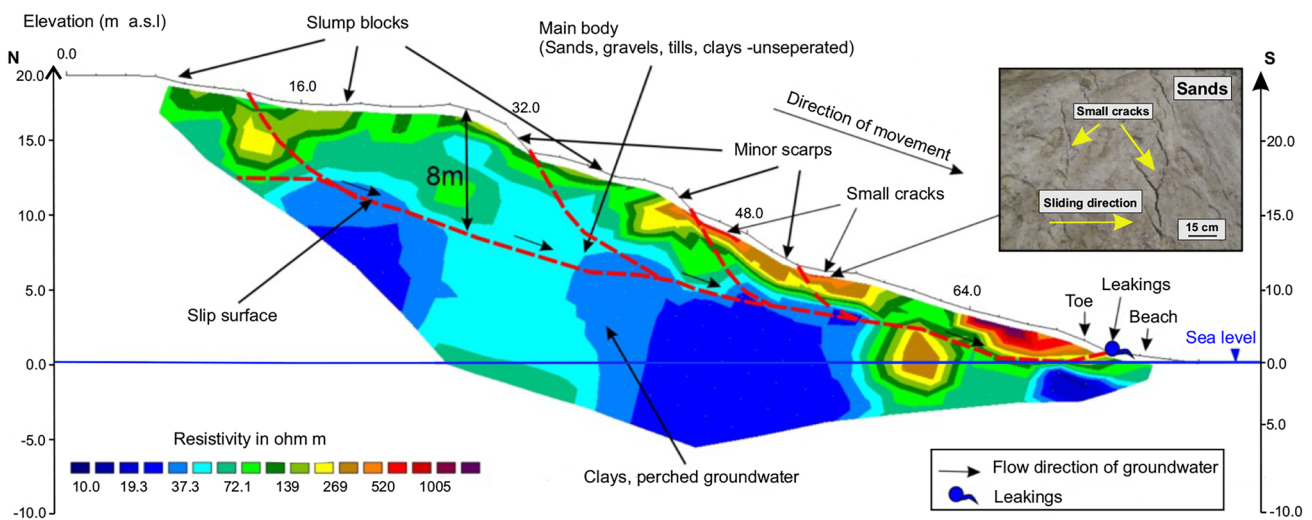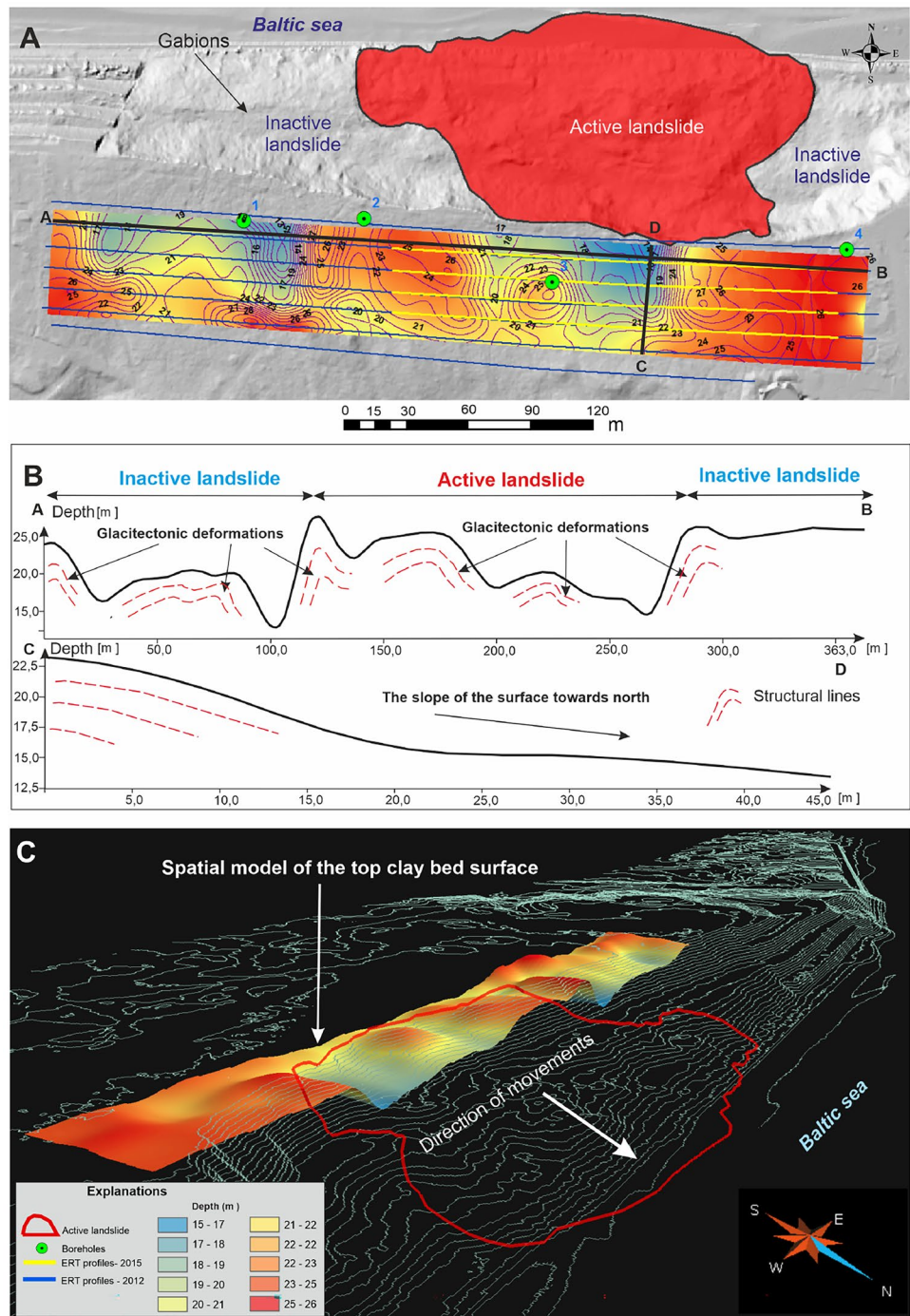

Fig. 19 Geological interpretation of the 2D ERT section

Fig. 20 A The top of clay bed surface relief model. **B** The lowest values of the height of the top of clay bed relief model occur in M and N areas (sections A–B). The C–D sections through region N show the significant slope of the top of clay bed top surface towards the north. **C** Spatial view on the top clay bed surface

the cliff, the gabions remained almost undamaged. There are two main reasons why this portion of the cliff (the intact gabion region) is not active today. The first reason is the geology. Upon analysing the data of 3D ERT models in conjunction with field observations, it was found that in this part of the cliff, there are more sand and gravel rock than clay components. They are poorly consolidated and not heavy. In contrast, in the area of the active landslide, in the vicinity of borehole 3, there are mainly thick, heavy tills. Groundwater occurring in the aeration zone destructively affects the stability of the cliff coast. They cause a weakening of the strength properties of tills, maintaining the stability of the cliff. The stability of the slope is reduced by also beds of glacial till and clay formations, which occur at the base of the cliff in the zone of sea level fluctuations.

The second reason is related to the destructive impact of groundwater on the cliff stability. In the area of an active landslide, the clay beds contain more perched groundwater than that found in the sand beds. Due to the low resolution of both 3D ERT models, narrow sand beds with perched groundwater may be difficult to interpret. This water makes the clay more plastic and therefore more susceptible to the formation of slip surfaces (Del Río et al. 2009; Greggio et al. 2018).

The composition and water content of rocks will also affect the interpretation of resistivity. The example described clearly demonstrates that processes involved within unconsolidated sedimentary cliff are both universal and include regional nuances that shed new light on bluff coast erosion and geodynamic development. Geophysics surveys play a prominent role in the evaluation of cliff stability since electrical resistivity is related to important bulk physical properties such as water content, clay content, lithology, and fracture density. These quantities are important factors that control the bulk strength of rock formations and hence the mass movement potential. Because one kind of geophysical method may have many interpretations, we recommend using comprehensive geophysical prospecting and boring to carry out the work.

Conclusions

This paper presents a comprehensive methodology recognizing the geology of cliff and landslide and determining their dynamics. For this purpose, multitemporal ALS data, ERT method, boreholes, and field studies in the context of landslide hazard were applied.

The application of multitemporal DTMs has shown itself to be a very useful method of studying the dynamics of cliff edges and landslide. In our study, the differential ALS models indicate that the landslide became active in 2010 after the occurrence of intense and prolonged rainfall in May and June 2010. A morphological cross-section made between the 2008 and 2020 ALS models shows that the cliff edge has receded a maximum of about 53 m over 12 years. Such large displacements of the cliff edges were detected in the area of the active landslide range. Electrical resistivity tomography (ERT) can be successfully implemented in cliff and landslide studies because it provides a lot of new detailed information about the geology of the cliff and structure of the landslide. In our work, ERT studies of landslides documented many high-resistivity cracks and made it possible to interpret the area of the slip surface and the flow direction of the groundwater. In order to understand and determine the reasons for such high dynamics of the cliff edge, two 3D ERT models of different sizes and resolutions were generated. The first model generated in 2012 allowed for preliminary identification of the geology. Thick beds of tills, sands, perched groundwater, and gravels bedding on the plastic clays were identified. Additionally, glacitectonic deformations were made evident in the top of clay. In the area of an active landslide, the second ERT model with a greater resolution showed more precisely the distribution of rock resistivity in the cliff. The difference between 2012 and 2015 ERT voxel models indicate that the rocks from the 2015 ERT model have a lower degree of water saturation than the rocks of the 2012 ERT model. By this means, it was possible to more accurately interpret the top of clay and the lithology of the rocks. Thus, the top of clay surface model was generated. New important information emerged from the analysis of the surface of this model. The relief is characterized by variable height difference (max 11.8 m)—which results from glacitectonic deformations of rocks. Such glacitectonic deformations had not been drawn on the geological cross-section previously (Fig. 2). The second important conclusion was that on the border with an active landslide (N-area), the fall of the top of the clay is directed north, i.e. towards the sea. Therefore, the thicker geological beds of heavy tills in this cliff region undergo dynamic sliding across the top of clay bed. We hold that active cliffs should be under continuous photogrammetric monitoring in order to capture the dynamics of changes in the relief of the cliff surface. At the same time, three-dimensional geophysical (preferably resistivity models) should be created for the most active parts of the cliffs. In order to predict further landslide movements, the results of photogrammetric and geophysical surveys should be linked with the measurement data from inclinometers and piezometers. The combined approaches described in this case study would be of interest to earth scientists, insurance companies, city planners, and government agencies working on landslide hazard in similar geomorphological settings. This paper is also relevant to those involved with risk studies related to landslides located in cliff areas. Further studies of the cliff will involve studying its dynamics using UAVs and geophysical monitoring.

Data availability The data that support the findings of this study are available from the corresponding author upon reasonable request.

Declarations

Conflict of interest The authors declare no competing interests.

References

Alpaslan N, Bayram M (2020) Landslide study with 2D electrical resistivity tomography (ERT): a case study from Turkey. Carpathian J Earth Environ Sci 15:391–403. https://doi.org/10.26471/cjees/2020/015/139

Axelsson P (2000) DEM generation from laser scanner data using adaptive TIN models. Int Arch Photogramm Remote Sens 33(B4/1):110–117

Baldi P, Fabris M, Marasella A, Monticelli R (2005) Monitoring the morphological evolution of the Sciara Del Fuoco during the 2002–2003 Stromboli eruption using multitemporal photogrammetry. J Photogr Remote Sens 59:199–211

Baldo M, Bicocchi C, Chiocchini U, Giordan D, Lollino G (2008) LiDAR monitoring of mass wasting processes: The Radicofani landslide, Province of Siena, Central Italy. Geomorphology 10:193–201

Bartnik A, Jokiel P (2012) Geography of floods and river floods (in Polish). Ed. University of Lodz

Bezerra M, Moura D, Ferreira Ã, Taborda R (2011) Influence of wave action and lithology on sea cliff mass movements in Central Algarve Coast, Portugal. J Coastal Res 275:162–171. https://doi.org/10.2112/JCOASTRES-D-11-00004.1

Dahlin T, Bernstone C, Loke MH (2002) A 3D resistivity investigation of a contaminated site at Lernacken. Sweden Geophysics 67(6):1692–1700

Dahlin T, Zhou B (2004) A numerical comparison of 2D resistivity imaging with 10 electrode arrays. Geophys Prospect 52(5):379–398

Davis JC (2002) Statistics and data analysis in geology. John Wiley & Sons, New York, Chichester, Brisbane, Toronto, Singapore

Del Río L, Gracia F, Benavente J (2009) Mass movements and cliff retreat along the SW Spanish coast. J Coastal Res 56:717–721

Derron MH, Jaboyedoff M (2010) LIDAR and DEM technique for landslides monitoring and characterization. Nat Hazards Earth Syst Sci 10:1877–1879

Dewez T, Rohmer J, Regard V, Cnudde C (2013) Probabilistic coastal cliff collapse hazard from repeated terrestrial laser surveys: case study from Mesnil Val (Normandy, northern France). J Coastal Res 65:702–707

Earlie CS, Masselink G, Russell PE, Shail RK (2015) Application of airborne LiDAR to investigate rates of recession in rocky coast environments. J Coast Conserv 19:831–845. https://doi.org/10.1007/s11852-014-0340-1

Emery KO, Kuhn GG (1982) Sea cliffs: their processes, profiles, and classification. GSA Bull 93(7):644–654. https://doi.org/10.1130/0016-7606(1982)93<644:SCTPPA>2.0.CO;2

Furmańczyk K (1994) Coastal zone of the Hel Peninsula in the light of a comprehensive analysis of satellite and aerial images, University of Szczecin, Scientific Papers Coastal zone of the Hel Peninsula in the light of a comprehensive analysis of satellite and aerial images (in Polish). Univ Szczecin Sci J

Gibb JG (1978) Rates of coastal erosion and accretion in New Zealand, New Zeal. J Mar Fresh 12:429–456. https://doi.org/10.1080/00288330.1978.9515770

Greggio N, Giambastiani BMS, Balugani E, Amaini C, Antonellini M (2018) High-resolution electrical resistivity tomography (ERT) to characterize the spatial extension of freshwater lenses in a salinized coastal aquifer. Water 10:1067. https://doi.org/10.3390/w10081067

Hackney C, Darby SE, Leyland J (2013) Modelling the response of soft cliffs to climate changes: a statistical, process-response model using accumulated excess energy. Geomorphology 197:108–121

Hapke CJ, Reid D, Richmond B (2009) Rates and trends of coastal change in california and the regional behavior of the beach and cliff system. J Coastal Res 253:603–615. https://doi.org/10.2112/08-1006.1

Hevesi JA, Flint AL, Istok JD (1992a) Precipitation estimation in mountainous terrain using multivariate geostatistics Part Istructural analysis. J Appl Meteorol 31:661–676

Hevesi JA, Flint AL, Istok JD (1992b) Precipitation estimation in mountainous terrain using multivariate geostatistics. Part II Isohyetal Maps J Appl Meteorol 31:677–688

Jacobsen PR, Overgaard T (2002) Georadar facies and glacitectonic structures in ice marginal deposits, northwest Zealand, Denmark. Quaternary Science Reviews, 21(8–9): 917–927. Available from: https://doi.org/10.1016/S0277-3791(01)00045-2

Jongmans D, Hemroulle P, Renardy F, Vanbrand Y (2000) Application of 2D electrical and seismic tomography techniques for investigating landslides. Eur J Environ Eng Geophys 8:75–89

Kamiński M (2011) Application of photogrammetric methods to assess the dynamics of mass movements – selected examples from Poland. Biul Państw Inst Geol 446:85–94

Kamiński M (2015) Application of airborne laser scanning and electrical resistivity tomography in comprehensive research of landslides – an example from the Dynów Foothill (Outer Carpathians). Prz Geol 63:410–417

Kamiński M, Krawczyk M, Zientara P (2012) Recognition of Geology of the Jastrzębia Góra Cliff Using Resistivity Tomography Methods for Landslide Hazard Biuletyn PIG-PIB 452:119–130

Kamiński M, Zientara P (2017) Geophysical model and displacement of active landslide—an example from Jastrzębia Góra Cliff (Northern Poland). In: Mikoš M., Arbanas Ž., Yin Y., Sassa K. (eds) Advancing culture of living with landslides. WLF 2017. Springer, Cham. https://doi.org/10.1007/978-3-319-53487-9_39

Kamiński M, Zientara P, Krawczyk M (2014) Application of resistivity tomography to study landslide the Dzianisz landslide (southwestern Podhale). Prz Geol 62:198–203

Kamiński M, Zientara P, Krawczyk M (2021) Electrical resistivity tomography and digital aerial photogrammetry in the research of the "Bachledzki Hill" an active landslide – in Podhale (Poland). Eng Geol 285 106004 ISSN 0013–7952. https://doi.org/10.1016/j.enggeo.2021.106004

Kramarska R, Frydel J, Jegliński W (2011) Terrestrial laser scanning application for costal geodynamice assesment: the case of Jastrzębia Góra cliff. Biuletyn PIG-PIB 446:101–108

Lapenna V, Lorenzo P, Perrone EA, Pisscitelli S, Sdao F, Rizzo E (2003) High-resolution geoelectrical tomographies in the study of Girrossa landslide (southern Italy). Bull Eng Geol Envirom 62:259–268

Lapenna V, Lorenzo P, Perrone A, Piscitelli S, Rizzo E, Sdao F (2005) 2D electrical resistivity imaging of some complex landslides in the Lucanian Apennine chain, southern Italy. Geophysics 70(3):B11–B18

Lee EM (2008) Costal cliff behavior: observations on the relationship between beach levels and recession rates. Geomorphology 101:558–571

Lidzbarski M, Tarnawska E (2015) The role of the hydrogeological research on cliff coast in diagnosis and forecasting of the geological hazard. Prz Geol 63:901–907

Ling C, Xu Q, Zhang Q, Ran J, Lv H (2016) Application of electrical resistivity tomography for investigating the internal structure of a translational landslide and characterizing its groundwater circulation (Kualiangzi landslide, Southwest China). J Appl Geophys 131:154–162. https://doi.org/10.1016/j.jappgeo.2016.06.003

Liu X, Petersen J, Zhang Z (2005) High-resolution DEM generated form LIDAR data for water resource management. Centre for GIS, Monash, Australia

Loke MH (2019) Tutorial: 2D and 3D electrical imaging surveys. http://geotomosoft.com. Accessed 31 Apr

Loke MH, Barker R (1996) Practical techniques for 3D resistivity surveys and data inversion. Geophys Prospect 44:499–523

Loke MH, Lane JW (2002) The use of constraints in 2D and 3D resistivity modelling. 8th Meeting of the European Section of the Environmental and Engineering Society, Aveiro, Portugal 4–5

Loke MH, Acworth I, Dahlin T (2003) A comparison of smooth and blocky inversion methods in 2D electrical imaging surveys. Explor Geophys 34:182–187

Majewski A, Dziadziuszko Z, Wiśniewska A (1983) Storm floods monograph 1951–1975. Wyd. Komunikacji i Łączności, Warszawa

Masłowska M, Zaleszkiewicz L, Olszak I, Jurys L Michałowska M (2002) Geology of Jastrzębia Góra cliff]. [In:] Zachowicz J, Kramarska R (Eds) [Geology of the Gdańsk region]. Polish Geological Institute, Gdańsk 59–62

Mora P, Baldi P, Casula G, Fabris M, Ghirotii M, Mazzioni E, Pesci A (2003) Global positioning systems and digital photogrammetry for monitoring of mass movements: application to the Ca' di Malta landslide (northern Apennines, Italy). Eng Geol 68:103–121

Overgaard T, Jakobsen PR (2001) Mapping of glaciotectonic deformation in an ice marginal environment with ground penetrating radar. J Appl Geophys 47(3–4):191–197. Available from: https://doi.org/10.1016/S0926-9851(01)00064-7

Pazzi V, Morelli S, Fanti R (2019) A review of the advantages and limitations of geophysical investigations in landslide studies. Int J Geophys 2983087:27. https://doi.org/10.1155/2019/2983087

Perrone A, Lapenna V, Piscitelli S (2014) Electrical resistivity tomography technique for landslide investigation: a review. Earth Sci Rev 135:65–82

Prémaillon M, Regard V, Dewez TJB, Auda Y (2018) Global Recession Rates of Coastal Cliffs: a Global Relational Database to Investigate Coastal Rocky Cliff Erosion Rate Variations Earth Surf Dyn 6:651–668

Rączkowski W (2019) History of landslide research in Poland. Prz Geol 67(5):288–290

Samodra G, Ramadhan MF, Sartohadi J et al (2020) Characterization of displacement and internal structure of landslides from multitemporal UAV and ERT imaging. Landslides 17:2455–2468. https://doi.org/10.1007/s10346-020-01428-0

Santarato G, Ranieri G, Occhi M, Morelli G, Fischanger F, Gualerzi D (2011) Three-dimensional electrical resistivity tomography to control the injection of expanding resins for the treatment and stabilization of foundation soils. Eng Geol 119:18–30

Skompski S (1999) Detailed geological map of Poland 1:50 000, sheet Puck. Wydawnictwa Geologiczne Warsaw

Skompski S (2001) Explanatory notes for detailed geological map of Poland 1:50 000, sheet Puck Wydawnictwa Geologiczne, Waraw 36

Subotowicz W (1982) Litodynamic of the Polish cliff coasts (in Polish). GTN Ossolineum, Wrocław 150

Subotowicz W (1989) Studies of the cliff coast in Jastrzębia Góra (in Polish). Technika i Gospodarka Morska 7(452):336–339

Subotowicz W (1991) Protection of the cliff coast between Jastrzębia Góra and Rozewie (in Polish). Inżynieria Morska i Geotechnika 4:143–145

Subotowicz W (2000) Geodynamic Studies of cliffs in Poland and the problem of the protection of the cliff in Jastrzębia Góra (in Polish). Inżynieria Morska i Geotechnika 5:252–257

Subotowicz W (2003) Landslides in the area of the former holiday resort "Horizon" and the protection of the cliff shore in Jastrzębia Góra (in Polish). Inż Mor 24:10–14

Subotowicz W (2015) The cliff shore in Jastrzębia Góra and numerous attempts to protect it (in Polish). Zesz Nauk Kujawskiej Szkoły Wyższej 41:19–27

Terefenko P, Giza A, Paprotny D, Kubicki A, Winowski M (2018) Cliff retreat induced by series of storms at Międzyzdroje (Poland). J Coastal Res 85:181–185. https://doi.org/10.2112/SI85-037.1

Technical delivery reports. Sea coast monitoring. Report on the work carried out in 2008-2020 Maritime Office in Gdynia. https://www.mediafire.com/folder/u95l9197wjsiv/Monitoring

Udphuay S, Günther T, Mark E, Everett Robert R, Warden J-LB (2011) Three-dimensional resistivity tomography in extreme coastal terrain amidst dense cultural signals: application to cliff stability assessment at the historic D-Day site. Geophys J Int 18(51):201–220. https://doi.org/10.1111/j.1365-246X.2010.04915.x

Uścinowicz G, Kramarska R, Kaulbarsz D, Jurys L, Frydel J, Przeździecki P, Jegliński W (2014) Baltic Sea erosion; a case study from the Jastrzębia Góra region. Geologos 20(4):259–268

Uścinowicz G, Jurys L, Szarafin T (2017) The development of unconsolidated coastal cliffs (Pobrzeże Kaszubskie, Northern Poland). Geol Quart 61(2):491–501. https://doi.org/10.7306/gq.1351

Wang CK, Tseng YH (2010) DEM generation from airborne LIDAR data by an adaptive dual-directional slope filter. In: ISPRS TC VII Symposium – 100 Years ISPRS, Vienna, Austria XXXVIII(Part 7B):628–632

Werno M (2010) Documentation of geotechnical investigations of the cliff in Jastrzębia Góra at km 134.270–134.477 covering test borings with soil sampling and laboratory tests to determine the physical parameters mechanical and mechanical ground. Arch Maritime Office in Gdynia

Whiteley JS, Chambers JE, Uhlemann S (2019) Geophysical monitoring of moisture-induced landslides: a review. Rev Geophys 57:106–145

Wróbel M, Stan-Kłeczek I, Marciniak A, Majdański M, Kowalczyk S, Nawrot A, Cader J (2022) Integrated geophysical imaging and remote sensing for enhancing geological interpretation of landslides within uncertainty estimation—a case study from Cisiec. Poland Remote Sens 15(1):328. https://doi.org/10.3390/rs15010238

Young AP, Ashford SA (2006) Application of airborne LIDAR for sea cliff volumetric change and beach-sediment budget contributions. J Coast Res 222:307–318. https://doi.org/10.2112/05-0548.1

Zaleszkiwicz L, Masłowska M, Koszka-Maroń D, Olszak (2000) The cliff at Jastrzębia Góra. In: Uścinowicz S, Zachowicz J (eds) Quaternary stratigraphy and the disappearance of the ice sheet in the Kashubian Lake District. VII Conference "Stratigraphy of the Pleistocene of Poland". Państw. Inst. Geol., Gdańsk, pp 117–119

Zhang W, Harff J, Schneider R, Wu C (2010) Development of modelling methodology for simulation of long-term morphological evolution of the southern Baltic coast. Ocean Dyn 60:1085–1114

Zhang W, Harff J, Schneider R, Meyer M, Wu C (2011) A multiscale centennial morphodynamic model for the Southern Baltic coast. J Coastal Res 27:890–917